THE ULTRAVIOLET ABSORPTION SPECTRUM OF THIONYLIMIDE

AND

THE ROTATIONAL ENERGY FORMULAE FOR LINEAR POLYATOMIC MOLECULES IN $^2\Sigma$ AND $^3\Sigma$ ELECTRONIC STATES IN WHICH ONE OR MORE QUANTA OF A DEGENERATE BENDING VIBRATION IS EXCITED

by

JOHN MICHAEL ALLEGRETTI

A.B. (Honors) University of California, Berkeley, 1969

A THESIS SUBMITTED IN PARTIAL FULFILMENT OF

THE REQUIREMENTS FOR THE DEGREE OF

MASTER OF SCIENCE

in the Department

of

Chemistry

We accept this thesis as conforming to the

required standard

THE UNIVERSITY OF BRITISH COLUMBIA

June, 1971

In presenting this thesis in partial fulfilment of the requirements for an advanced degree at the University of British Columbia, I agree that the Library shall make it freely available for reference and study. I further agree that permission for extensive copying of this thesis for scholarly purposes may be granted by the Head of my Department or by his representatives. It is understood that copying or publication of this thesis for financial gain shall not be allowed without my written permission.

Department of Chemistry

The University of British Columbia
Vancouver 8, Canada

Date July 6, 1971

ABSTRACT

Thionylimide, HNSO, was prepared and its ultraviolet spectrum recorded for the first time. Two transitions are seen; a long series of bands in the 2700Å region and a continuum ending at approximately 3440Å. Franck-Condon overlap calculations were carried out to ascertain how large a shape change was occurring in the 2700Å system. Reasons for the diffuse nature of the bands in the 2700Å system and the continuous nature of the absorption in the 3440Å region are given.

In the second part of this thesis, formulae for the rotational energies of linear polyatomic molecules in $^2\Sigma$ and $^3\Sigma$ electronic states in which one or more quanta of a degenerate bending vibration are excited are derived. It is found in $^2\Sigma$ electronic states that the spin doubling and the ℓ-type doubling are independent provided the rotational constant B is much larger than γ, the spin rotation constant. In $^3\Sigma$ electronic states departures from the normal triplet spin pattern occur at low N values, when the vibrational angular momentum is still mainly coupled to the axis of the molecule. The effect is enhanced if λ, the spin-spin interaction constant, is large compared to B. At high N values the normal triplet pattern is approached as the vibrational angular momentum is uncoupled from the axis of the molecule.

TABLE OF CONTENTS

List of Tables and Figures

ACKNOWLEDGMENT

The author wishes to thank Dr. A.J. Merer for his advice and encouragement in carrying out the research which this thesis is based on and during the writing of this thesis. The author also wishes to thank Peter Tchir and Dr. R.D. Spratley for providing matrix isolation infra-red spectra of thionlyimide and their help with the vibrational analysis programs, and last but not least, E.J.F. who gave quite a hand in putting this thesis together.

INTRODUCTION

This thesis consists of two parts which are basically unrelated. The first part deals with the molecule thionylimide (HNSO or DNSO) and its ultraviolet spectrum. This study is prompted by the fact that the first strong ultraviolet absorption system of the isoelectronic molecule SO_2 has yet to be analyzed, despite many attempts (1,2). It is reasoned that, thionylimide being isoelectronic with SO_2 and having a similar shape, an understanding of the ultraviolet spectrum of thionylimide would help decipher the 2900Å system of SO_2. In the end, though, due to the lack of information available from the thionylimide spectrum resulting from its diffuseness, the opposite occurred and preliminary results from SO_2 were used to help explain the ultraviolet absorption spectrum of thionylimide.

In this thesis there is described the preparation of thionylimide and the first observation of its ultraviolet spectrum. Two absorptions have been seen: a long series of diffuse bands in the 2700-2100Å region and a continuum at longer wavelengths. Franck-Condon overlap calculations were carried out for the 2700Å system to see how large a shape change is necessary to explain the observed spectrum, and whether this shape change correlates with the shape change occurring in the 2900Å system of SO_2. Reasons for the diffuseness of the bands in the 2700Å system and the continuous nature of the long wavelength system are given based on

the electronic structure of thionylimide.

The second part of this thesis deals with the derivation and discussion of rotational energy formulae for linear polyatomic molecules in doublet and triplet Σ electronic states in which one or more quanta of a degenerate bending vibration are excited. As yet, no theoretical treatment exists for this topic(3), though with the advent of flash photolysis techniques, several examples of such molecules are now known. In particular, a system of HCCN at 3200-3400Å, which is probably a $^3\Sigma^- - {}^3\Sigma^-$ transition, shows vibrational "hot" bands in the H-C-C degenerate bending vibration which have so far defied rotational analysis according to the conventional energy level formulae for $^3\Sigma$ states (4).

The hamiltonian has been written in "effective" form (i.e. writing the electron spin interactions as parameters to be determined experimentally) and its matrix elements given in a Case (a) representation correct to second order. The results have been given in Case (b) notation for some cases of interest. The results are discussed in relationship to what would be seen in actual molecules.

CHAPTER I

THE ULTRAVIOLET SPECTRUM OF THIONYLIMIDE

1-1 Experimental

a. Preparation of HNSO and DNSO

The commonest methods of making thionylimide are the hydrolysis of NSF and the direct gas phase reaction of NH_3 and $SOCl_2$ (5,6). In all experiments reported here, thionylimide was produced by the latter method. This was because the starting material was readily available and results in a purer product than by the hydrolysis of NSF.

Since SO_2 is always formed as a by-product during any preparation of thionylimide, one must be extremely careful to choose conditions which minimize the amount of SO_2 formed, since SO_2 absorbs throughout the ultraviolet. Kirchhoff (7), during his microwave studies of thionylimide, discovered that thionylimide could be prepared reasonably free of SO_2 by using low pressures of NH_3 and $SOCl_2$ in the exact stoichiometric proportions for the reaction

$$3NH_3 + SOCl_2 \rightarrow 2NH_4Cl + HNSO \qquad (1)$$

Higher pressures of reactant gases resulted in a higher percentage of SO_2 produced. Accordingly, Kirchhoff's conditions, 12 torr NH_3 and 4 torr $SOCl_2$, were followed for all experiments. It was

found that the amount of SO_2 impurity produced was very sensitive to traces of water present in the apparatus or reagents (presumably from the direct hydrolysis of $SOCl_2$). Thus the glass apparatus had to be well flamed under vacuum prior to the preparation, and the ammonia had to be carefully dried over sodium metal. $SOCl_2$ was purified by trap to trap distillation to remove SO_2, HCl, and dissolved air. It was never possible to prevent the formation of SO_2 entirely, and an average sample of thionylimide contained 5% SO_2 as judged from the ultraviolet spectrum. This is presumably because reaction (1) is not the only reaction occurring (5,6). A major difficulty with preparation of HNSO is that whenever the gas is trapped in dry ice or liquid nitrogen, it immediately polymerizes. It is thus not possible to purify HNSO by fractional distillation (see below).

DNSO was prepared in an analogous way to HNSO except that ND_3 was used. The heavy ammonia was both prepared in the lab and obtained from a cylinder. The ND_3 prepared in the lab was synthesized using Mg_3N_2 and D_2O in the following reaction (8):

$$6\ D_2O + Mg_3N_2 \longrightarrow 2\ ND_3 + 3\ Mg(OD)_2 \qquad (2)$$

In the preparation an excess of Mg_3N_2 is used to produce a very dry sample of ND_3. The D_2O used was from Stohler Isotopes (99.8% D). The Mg_3N_2 was from Alpha Inorganics and had to be heated in vacuo prior to use to remove "light" water hydroxides. The bottled ND_3 was from Merck, Sharpe, and Dohme and was 99% D.

The samples of DNSO prepared were ascertained to be at least 70% D using matrix infra-red techniques.

b. Apparatus and preparative method

The thionylimide was prepared in a standard all glass vacuum line incorporating either a six or two twenty-two liter reaction vessels and a U tube trap (see fig. 1). Pumping was by means of a rotary pump and an oil diffusion pump. Pressures were measured with a thermocouple gauge and a manometer filled with Dow Corning 707 silicone fluid (12.8 mm oil = 1 mm Hg).

The actual preparation of thionylimide involved first filling the reaction vessel with dry ammonia to the correct pressure and then trapping the ammonia out in the U tube trap with liquid nitrogen. The reaction vessel was then filled with $SOCl_2$. The ammonia was then evaporated back into the reaction bulb where it reacted immediately with the $SOCl_2$, forming a yellow-white coating mostly of NH_4Cl on the glass walls.

c. Identification and analysis of reactant products

Positive identification of the gas produced as thionylimide was accomplished by infra-red and mass spectrometric techniques. The infra-red spectrum was taken of a matrix isolated sample at 4^oK. The thionylimide was diluted with argon in the ratio of 1:800. Samples were deposited at 120 microns pressure on a CsI window. [See ref. (9) for a complete description of the matrix isolation technique.] Spectra were taken on a Perkin-Elmer 225 infra-red spectrophotometer. The matrix isolated spectrum was identical with

the gas phase spectrum except for small shifts caused presumably by interactions with the matrix, and the absence of rotational structure (see fig. 10).

The mass spectrum of thionylimide was taken on a MS 9 mass spectrometer. The mass spectrum showed a weak parent ion peak at m/e = 63 $(HNSO^+)$ and another peak at m/e = 15 $(NH)^+$. There was a strong peak at m/e = 48 $(SO)^+$, but the SO^+ may have come from SO_2 for there was also a strong peak at m/e = 64 $(SO_2)^+$.

d. Notes on other attempts to prepare pure thionylimide

Attempts to produce large pressures of thionylimide by condensing successive batches in a trap and reconstituting the monomer from the polymer by heating the trap to 70°C as reported by Schenk (10) only yielded large amounts of SO_2 and very little thionylimide. It had been hoped that HNSO free of SO_2 could be produced by this method, but it turned out that Schenk's results could not be reproduced at all.

e. Spectroscopic experiments

Preliminary ultraviolet spectra were taken on a Bausch and Lomb 1.5 meter Eagle spectrograph, the experimental arrangements having been as in fig. (2). The lamp shown in fig. (2) was a P.E.K. 75 watt high pressure xenon lamp. The one lens shown focused an image of the lamp on the slit. The cell shown is a 75 cm all quartz cell with Suprasil windows. With a 60 μ slit and cell pressures ranging from 4 to ∿ 0.2 torr, exposure times were of the order of 4 seconds using Kodak SA-I film. For

calibration a 25 m.a. Westinghouse Iron hollow cathode lamp was used.

Higher resolution spectra (approximately 150,000 resolving power) were taken in the second order of a 21 ft. Eagle spectrograph as shown in fig. (3) with the previously mentioned light source and cell. To lower the exposure times, a 22.5 cm focal length cylindrical lens was used to focus the image of the arc on the slit as a line. A Corning 9-54 filter placed between the lamp and the cell was used to prevent photolysis of thionylimide. With a 20 μ slit and cell pressures ranging from 4 torr to less than 0.1 torr, and using Kodak SA-I plates, exposures were of the order of two minutes. Calibration was with a 120 m.a. iron hollow cathode lamp of the lab's own design. In these experiments a moderately intense, but diffuse, band system lying in the region 2700-2100$\mathring{A}$ (to be discussed below) was discovered.

Temperature studies of the bands of this system were carried out using the same experimental arrangement as above except that the cell was wrapped with heating tape. The cell temperature was controlled by regulating the applied voltage to the heating tape. The cell was heated in 25^{o} steps to a maximum of $100^{o}C$. The cell temperature was monitored using a Chromel-Alumel thermocouple in conjunction with a Leeds and Northrup millivolt potentiometer.

The next experiment was a search for weaker transitions of thionylimide at longer wavelengths in the 3600 $\mathring{A}$ region. To do

this a 4 meter White type (11) multiple reflexion cell was built and used in conjunction with a reaction vessel consisting of two twenty-two liter globes. The cell was constructed of 85 mm pyrex tubing, to the ends of which 6 inch sections of 3 inch diameter pyrex pipe end-pieces with O-ring grooves were blown on. Normal pyrex pipe flanges were used to attach the end plates which sealed the cell (see fig. 4). One cell end-plate carried the Suprasil entrance and exit windows, while the other had the external controls for the D mirrors. Inserted in the cell was a"boat" to the front of which was attached the "shouldered" mirror. The number of traversals of the cell was controlled by manipulation of the D mirrors.

The cell was set up as in fig. (4) using the previously mentioned lamp. Care had to be taken so that the incoming cone of light matched the aperture of the White cell so as not to produce stray light reflected off the inside walls of the cell (cone too large) or to underfill the D mirror (cone too small). This critical adjustment was done by moving the 35 cm lens shown in fig. (4) relative to the light source. After the light had passed through the White cell, a 55 cm cylindrical lens focused the light on the slit of the spectrograph. Corning 0-56 and 7-54 filters were used to stop photolysis of the sample by light with a wavelength less than 3000Å, which was found to produce decomposition products on the mirrors unless it was eliminated. With the White cell set for 24 traversals, or an effective path length of 96 meters, and a 80 μ

main slit, exposures were of the order of four minutes using Kodak IIa-O plates and cell pressure ranging from 2.6 torr to 0.23 torr. The 120 m.a. iron hollow cathode lamp was again used for calibration.

The White cell was also used to look at the weak "tail" of the 2700Å system of thionylimide. The cell was set up as previously described except that the Corning filters were replaced with an order separator in front of the main slit, consisting of a foreslit, concave mirror, and quartz prism (see fig. 4). The order separation was necessary because the filters could not completely eliminate the intense overlapping first order radiation ($\lambda \sim 5200$Å) from the xenon arc. Using Kodak I-D film, an 80 μ main slit, a 2 mm foreslit, gas cell pressures of the order of 0.2 torr, and 4 traversals, exposures were of the order of 5 to 10 minutes. Calibration was as previously described.

None of the White cell experiments were repeated with DNSO, and for DNSO only the 2700Å system was photographed. Measurements were made from contact prints of the plates. These are probably good to $\pm$ 25 cm^{-1}.

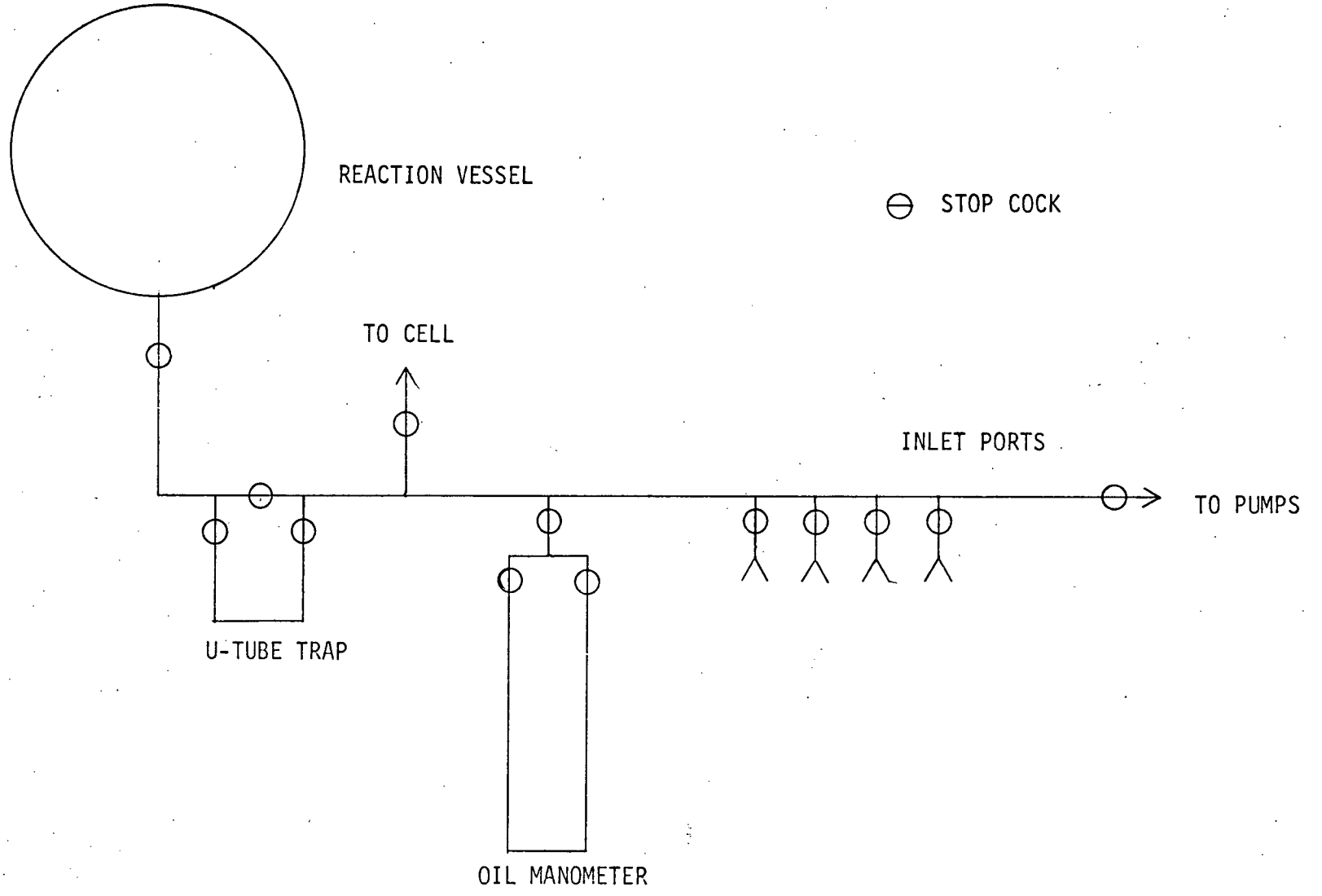

FIG. 1 THIONYLIMIDE PREPARATION SYSTEM

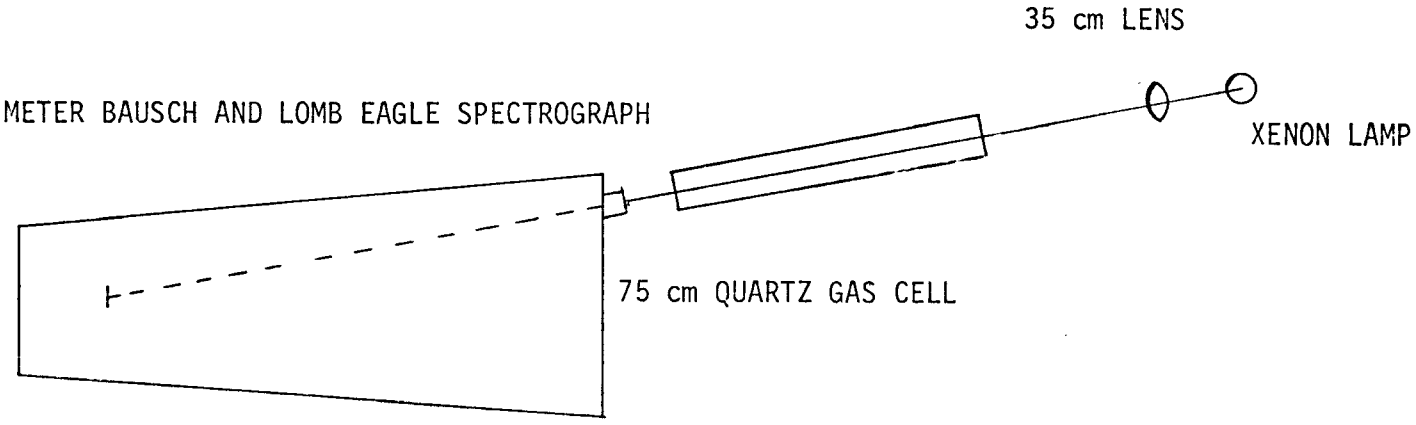
35 cm LENS
1.5 METER BAUSCH AND LOMB EAGLE SPECTROGRAPH
XENON LAMP
75 cm QUARTZ GAS CELL

FIG. 2

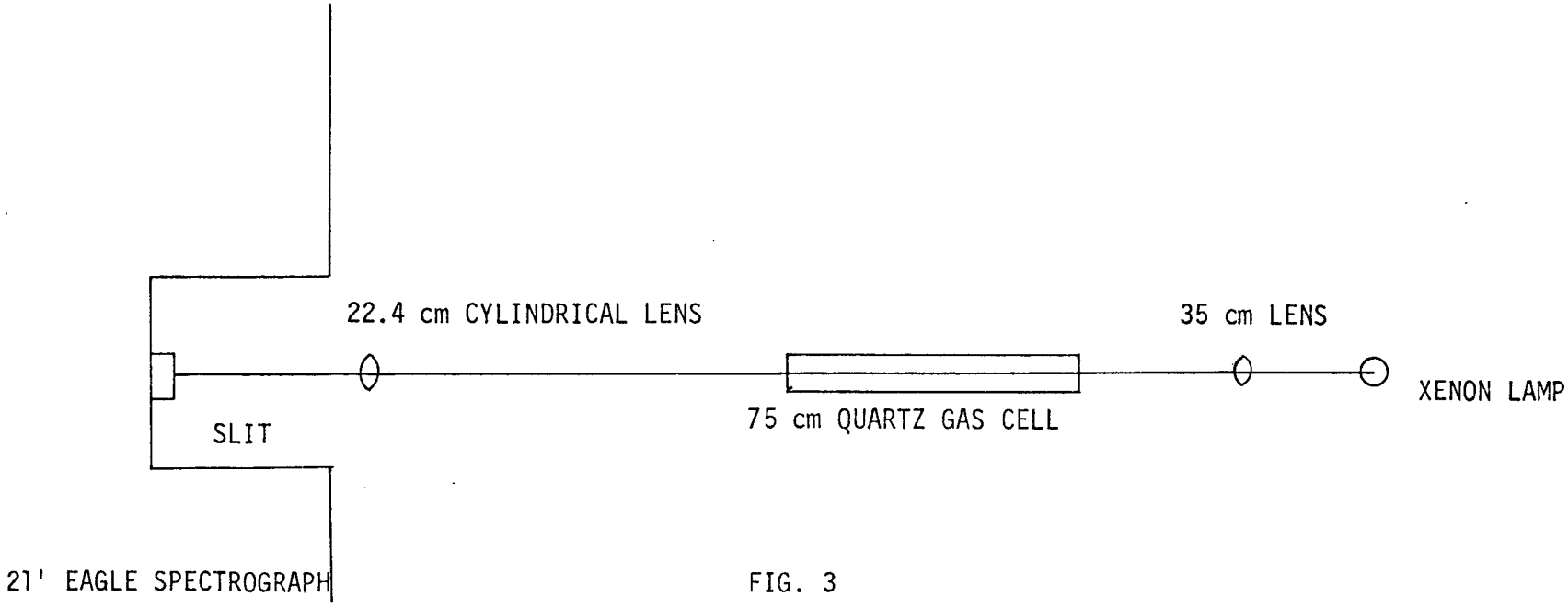
22.4 cm CYLINDRICAL LENS
35 cm LENS
XENON LAMP
SLIT
75 cm QUARTZ GAS CELL
21' EAGLE SPECTROGRAPH

FIG. 3

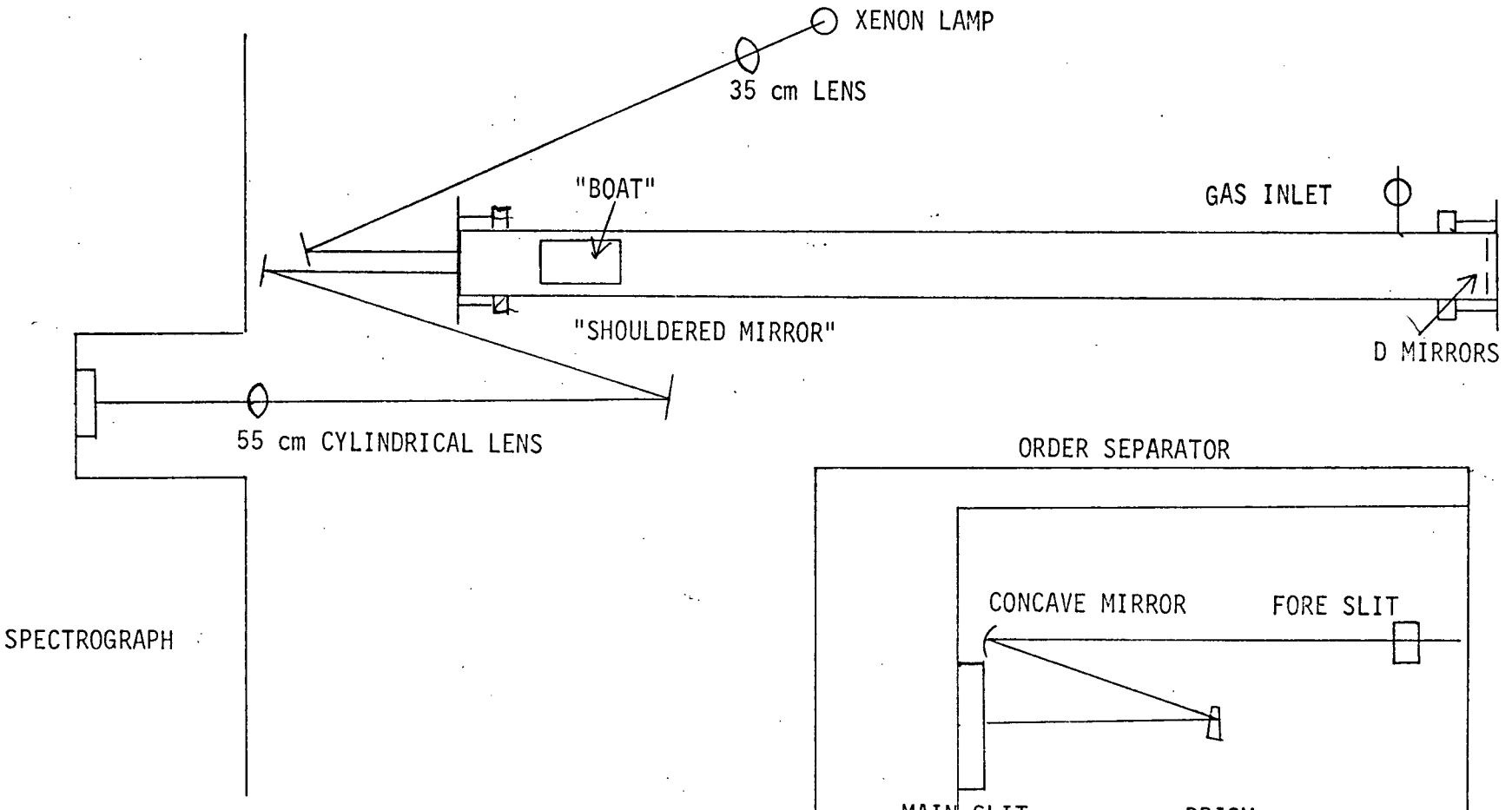

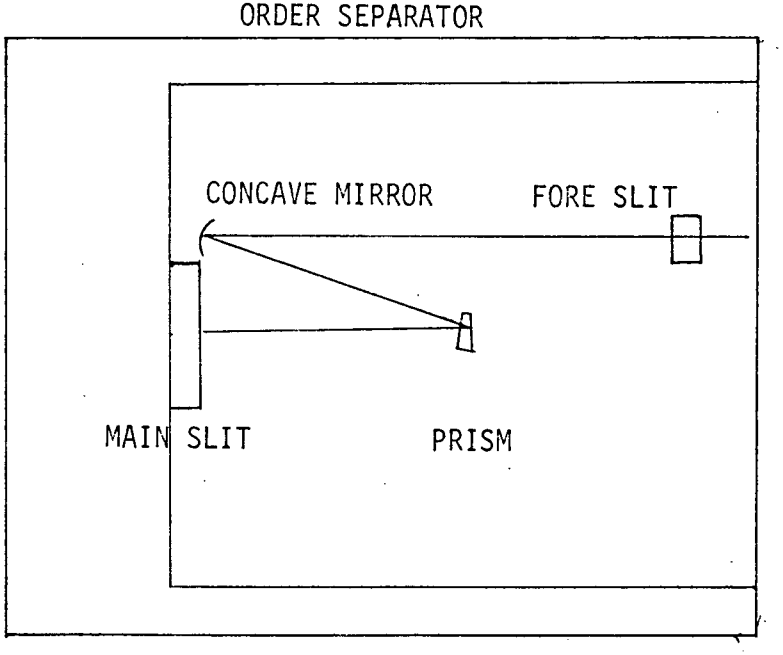

FIG.(4)4 METER WHITE CELL AND 21' EAGLE SPECTROGRAPH

1-2 Results

Low resolution absorption spectra of thionylimide taken on a Cary Model 14 spectrophotometer show moderately strong absorption in the 2700-1900Å range (see fig. 5,6,7). The absorption maximum comes at 2170Å; the system obviously continues past 1900Å but could not be observed for experimental reasons. On the long wavelength side of the absorption maximum the system loses intensity rapidly and is no longer discernible at 2700Å where it is lost under the tail of the strong 2900Å system of SO_2 (see fig. 6). The main features of the Cary spectra are a long series of absorption bands at the long wavelength end of the system, which can be followed from 2689Å to 2387Å (see fig. 5,6,7). The bands are most distinct at lower energies and, at the absorption maximum, they are no longer discernible.

At high resolution the bands noted above were found to be entirely diffuse, not even showing any partially resolved rotational structure (see fig. 8). The band positions are given in Table (1). Upon examination of Table (1), one will notice that the bands are not regularly spaced and cannot be fitted into a single progression.

The 2700Å system of DNSO showed several distinct differences from that of HNSO. The bands which stood out well in the spectra of HNSO no longer do so in DNSO (compare fig. 5 and 6). The bands in DNSO appear not to have been shifted to any great extent,

though new bands at 2543Å and 2530Å have appeared and the band that was at approximately 2535Å in HNSO has disappeared. The band that was 2517Å in HNSO has been shifted to 2515Å in DNSO. The other bands in the spectrum of DNSO do not appear to have changed position relative to the bands in the spectrum of HNSO.

The high resolution spectra of the 2700Å system of HNSO showed three very weak bands between the bands of the main progression. Due to the lack of contrast in the DNSO spectrum, the corresponding bands could not be seen. Upon heating the cell, these weak bands of HNSO appeared to gain intensity relative to the other bands as the cell temperature rose, thus showing them to be "hot" bands arising from excited vibrational levels in the ground state. Since the bands of the main progression did not change in intensity, they are "cold" bands.

The long path experiments in the 3400Å region did not disclose any sharp or banded absorption of HNSO but only a continuum beginning at approximately 3440Å (see fig. 9). Since $SOCl_2$ also has continuous absorption near this region,it was necessary to show that the two continua were not identical. Comparison of the new continuous absorption and spectra of $SOCl_2$ taken under similar conditions showed that the two continua were not the same. There are no other species involved in the preparative reaction that have a continuous absorption in the ultraviolet.

The long path experiments in the 2685Å region did not reveal any new bands in the tail of the 2700Å system of HNSO but

did verify the existence of a band at 2686Å. From 2686Å and to longer wavelengths, the 2900Å system of SO_2 rises in intensity and it becomes impossible to separate the weak and diffuse HNSO bands from the strong, sharp SO_2 absorption.

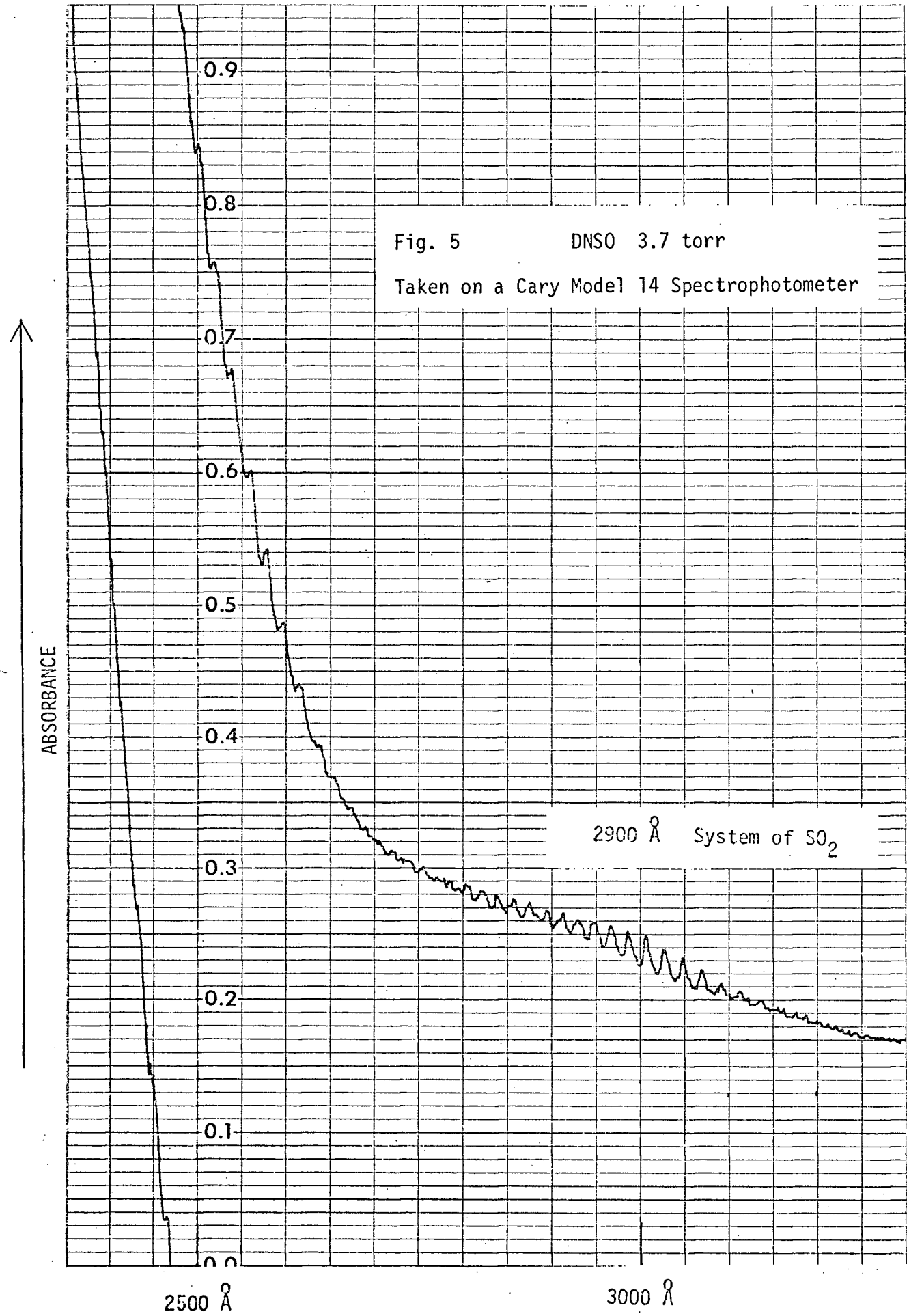

Fig. 5 DNSO 3.7 torr

Taken on a Cary Model 14 Spectrophotometer

2900 Å System of SO_2

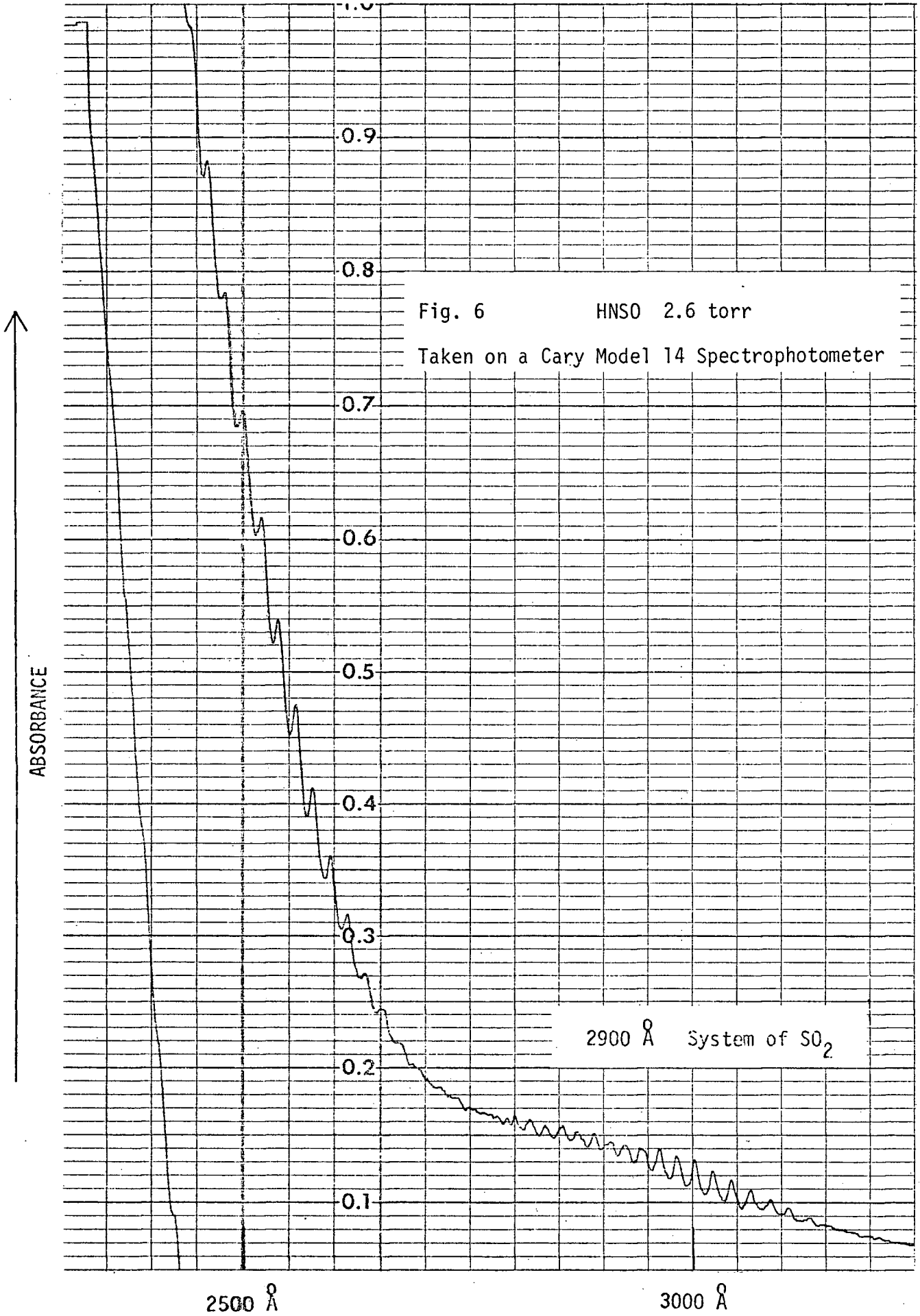

Fig. 6 HNSO 2.6 torr

Taken on a Cary Model 14 Spectrophotometer

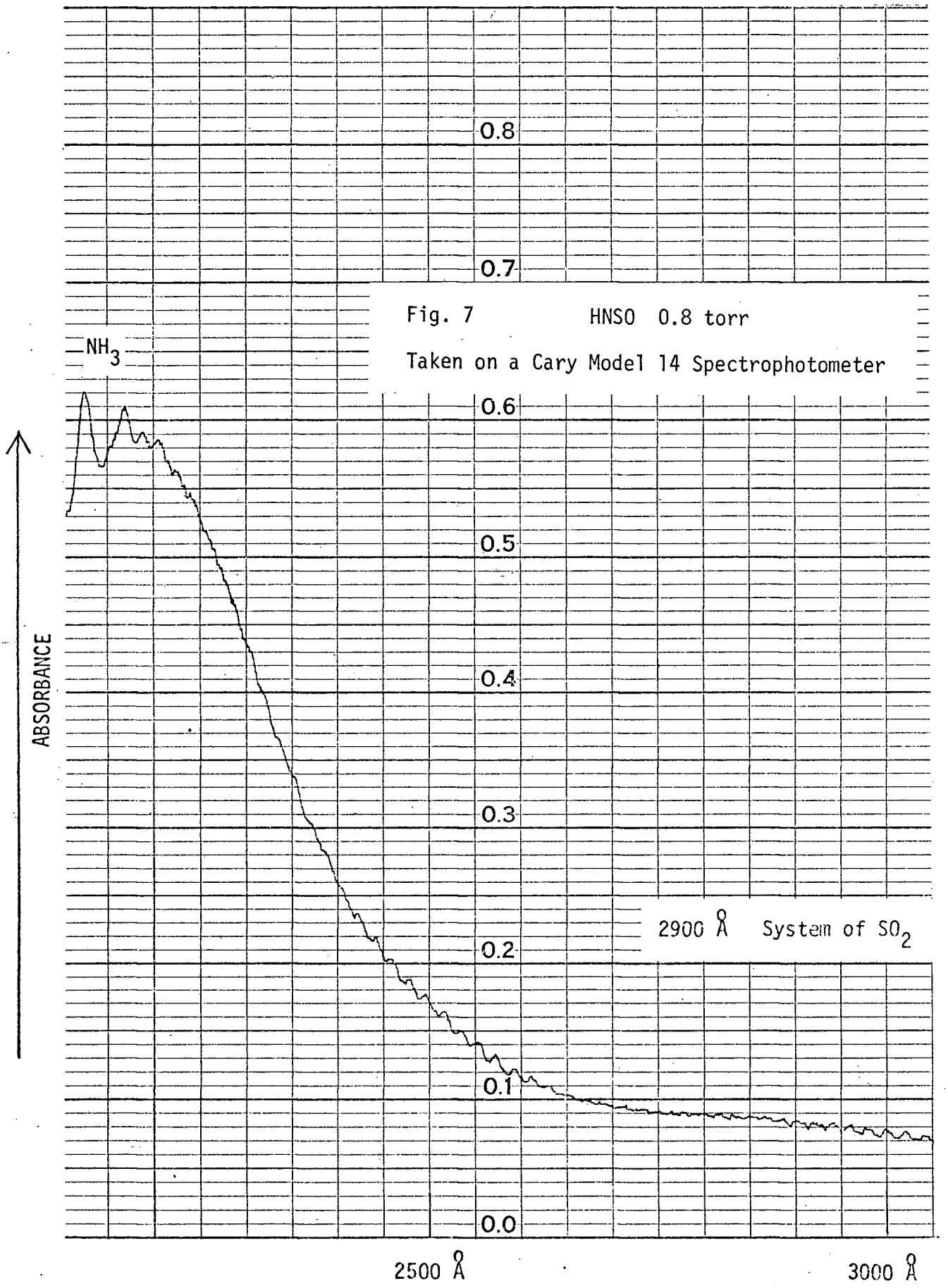

Fig. 7 HNSO 0.8 torr

Taken on a Cary Model 14 Spectrophotometer

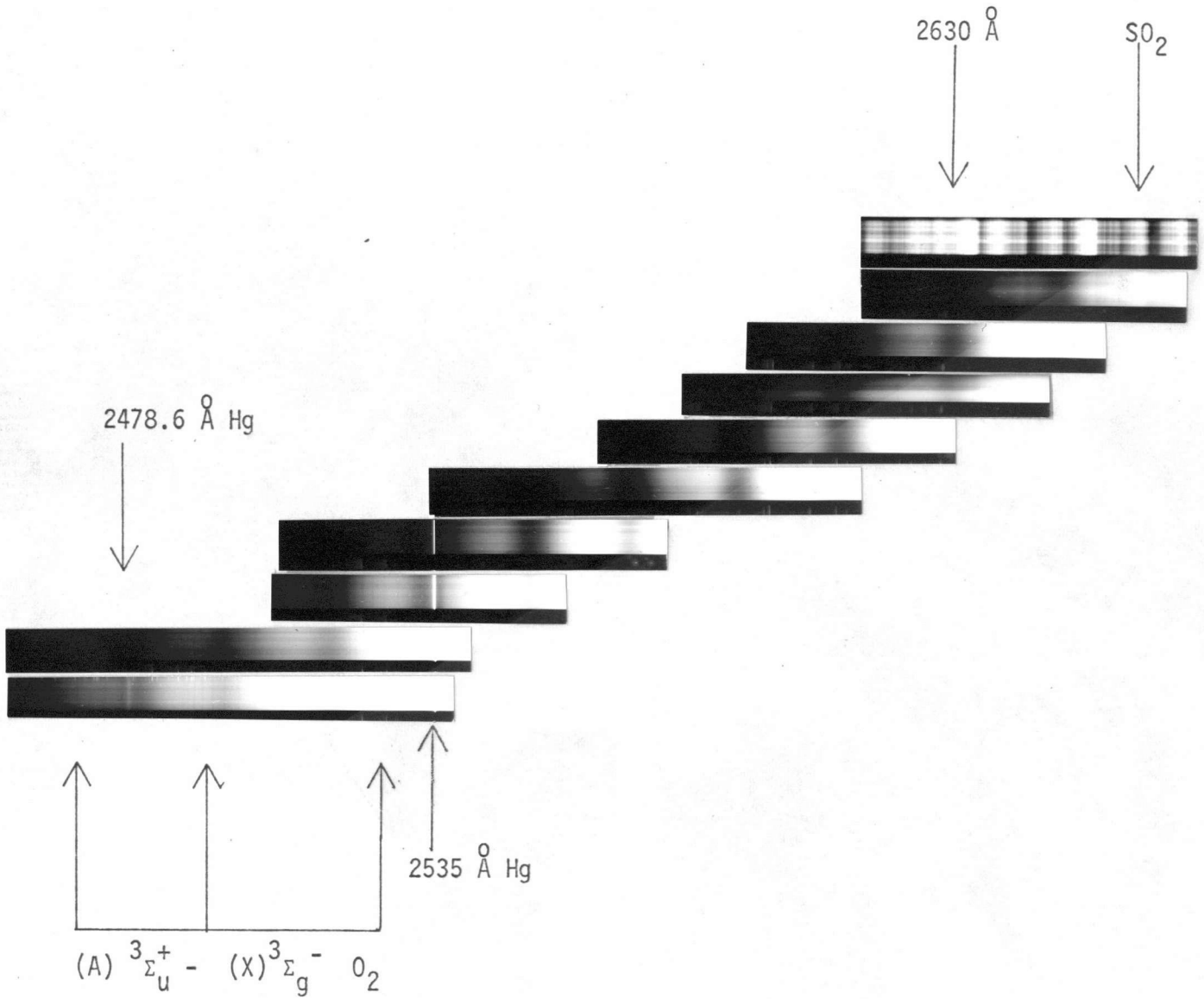

FIG. 8 The 2700 Å System of HNSO taken on a 21' Eagle Spectrograph

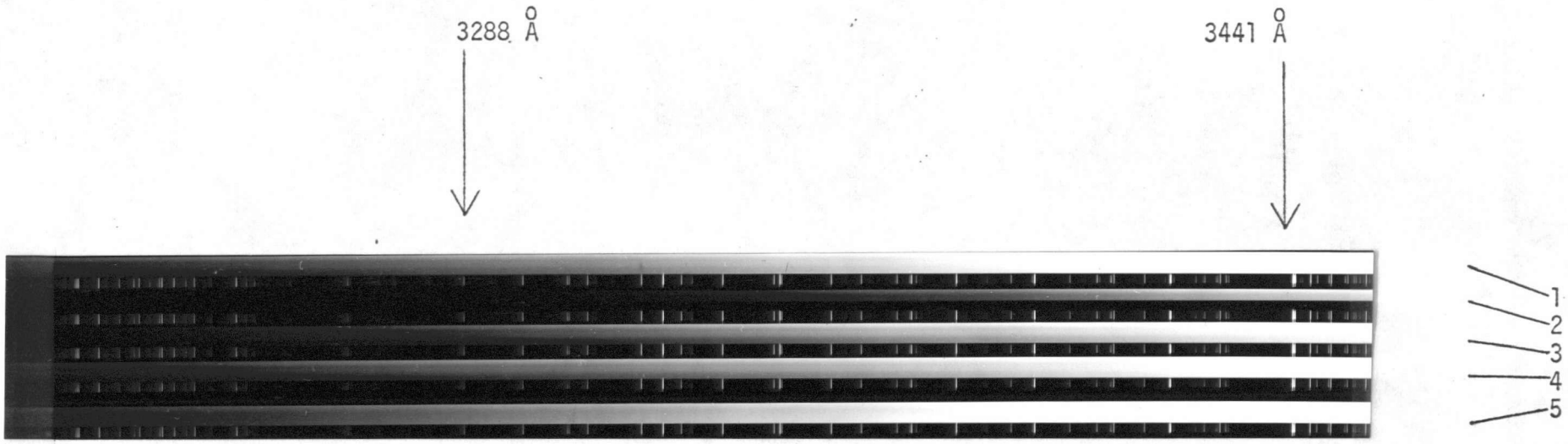

1,5 Cell empty
2 2.6 torr
3 0.7 torr
4 0.23 torr

FIG. 9 The 3440 Å Continuum of HNSO taken on a 21' Eagle Spectrograph in conjunction with a 4 meter White Cell set for 24 traversals

TABLE 1

A. HNSO Bands of the 2700Å system

	λ Obs.	Δλ Vac.	λ Vac.	ν Vac.
	2689.23 Å	0.80 Å	2690.03 Å	37174 cm^{-1}
	2671.82	0.79	2672.61	37417
	2652.14	0.79	2652.93	37694
	2636.25	0.79	2637.04	37921
*	2620.51	0.78	2623.29	38120
	2612.59	0.78	2613.37	38265
*	2603.92	0.78	2604.70	38392
	2593.46	0.78	2594.24	38544
*	2583.80	0.77	2584.57	38691
	2572.86	0.77	2573.63	38856
	2555.23	0.77	2556.00	39124
	2535.53	0.76	2536.29	39428
	2517.03	0.76	2517.79	39717
	2496.80	0.75	2497.55	40039
	2479.70	0.75	2480.45	40315
	2458.55	0.74	2459.29	40662
	2443.71	0.74	2444.45	40909
	2423.28	0.74	2424.02	41254
	2407.81	0.73	2408.54	41519
	2386.76	0.73	2387.49	41885

B. DNSO BANDS

2635.31	0.79	2636.10	37935
2612.23	0.78	2613.01	38270
2606.78	0.78	2607.56	38550
2573.36	0.77	2574.13	38848
2556.70	0.77	2557.47	39127
2543.14	0.76	2543.90	39310
2530.08	0.76	2530.84	39513
2515.10	0.76	2515.86	39748

*HOT BANDS

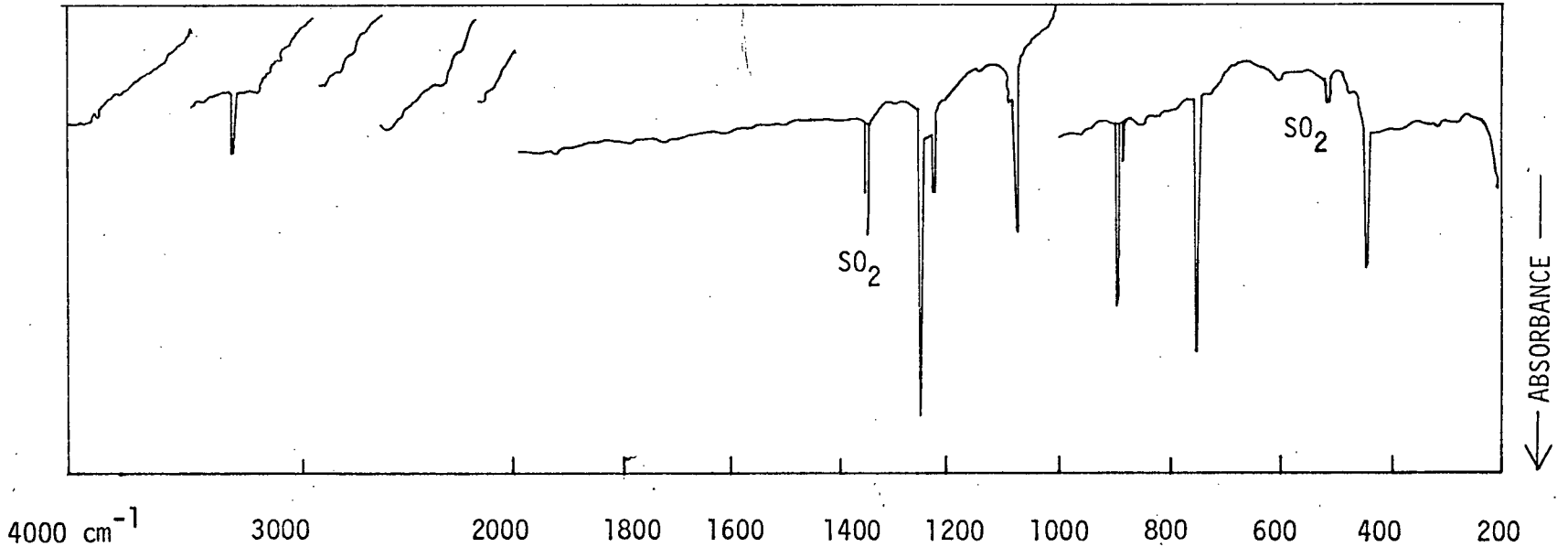

FIG. 10 Infra-Red Spectrum of Matrix Isolated HNSO taken on a Perkin-Elmer 225 Spectrophotometer at $4^{o}K$

1-3 Discussion and Interpretation of Results

As stated in the introduction, the reason for interest in thionylimide is its similarity with SO_2. In the following discussion, arguments will be made to further this point and results from SO_2 will be applied to thionylimide to help explain the observed results.

a. Ground state normal coordinates

To understand the 2700 Å system of thionylimide and the vibrations active in the system, one must first determine the normal modes of vibration in the ground state of the molecule. Richert (12), in his normal coordinate analysis, treated thionylimide as a triatomic molecule with the N-H group as a single atom. He used the set of diagonal force constants given in Table (2). For this work, a full normal coordinate analysis using a full set of diagonal force constants (that is neglecting all interaction force constants) was carried out. The normal coordinate analysis was carried out using the computer programs written by Schachtschneider (13). The force constants were varied until the calculated frequencies of HNSO, DNSO, $HN^{34}SO$, and $DN^{34}SO$ agreed to within approximately 5 cm^{-1} of the observed matrix isolation frequencies except for the vibrations involving a hydrogen atom. No attempt was made to refine the force constants to achieve a better fit of the calculated frequencies due to the problem with anharmonicity and matrix effects (see below). The final force constants are shown in Table(2),along with the

observed and calculated frequencies. The large errors in the calculated HN stretching and HNS bending vibrational frequencies can be attributed to anharmonic effects which are always large in molecules of this type. The anharmonic effects arise from the fact that the H and D "sample" different parts of the vibrational potentials and thus the anharmonicity affects them quite differently. No attempt was made to correct the observed frequencies for anharmonicity to get a better fit. Table(2) includes the resulting matrices $\underline{L}$ and $\underline{L}^{-1}$, where $\underline{L}$ is the matrix that transforms the vector of normal coordinates $\underline{Q}$ to internal coordinates $\underline{S}$, by the equations

$$\underline{S} = \underline{L}\underline{Q} \qquad (1)$$

or, in reverse,

$$\underline{Q} = \underline{L}^{-1}\underline{S} \qquad (2)$$

See Appendix 1 for a discussion of the formalism of the FG matrix methods of Wilson, Decius, and Cross (14).

b. Franck-Condon calculation for the bands of the 2700Å region

Now that the form of the normal coordinates in the ground state is known, one can use the Franck-Condon principle to determine what vibrations are active in the transition and how large a shape-change is necessary to explain the observed transition. The basis of the Franck-Condon principle is that the electronic transition in a molecule is assumed to take place so rapidly compared to the vibrational motion that the internuclear distance can be regarded

as fixed during the transition (15). Translated into quantum mechanical language, the strongest vibrational transitions according to the Franck-Condon principle are those with the largest values of the Franck-Condon overlap integral R_{MN}, defined as

$$R_{MN} = \int \psi_M' (Q') \quad \psi_N'' (Q'') \, dQ' \tag{3}$$

where ψ_M' and ψ_N'' are the vibrational wave functions in the upper and lower electronic states respectively. The relative intensity of a given band (M,N) in the electronic transition is equal to the square of this integral. Thus one is correlating an "overlap" between the upper and lower electronic state vibrational wave functions to the intensity of a given band.

As noted previously, the 2700Å system of thionylimide consists of a long series of bands that did not undergo any great change upon deuteration, though the bands did lose much of their intensity relative to the background. From the fact that a long series of bands is observed, one knows from the Franck-Condon principle that a large change of shape is occurring in the transition. From the fact that the observed series of bands is relatively insensitive to deuteration, one can say that the vibrations active in the transition, and therefore the shape change, do not involve the hydrogen atom and are centered in the S-O end of the molecule. See Table (2) for a comparison of the ground state HNSO and DNSO frequencies. To get some idea of which vibrations might be strongly active in the electronic transition and how much of a change of shape would be necessary to

produce the observed absorption maximum, several rough Franck-Condon overlap calculations were done.

Integrals of the type shown in eq. (3) were first evaluated by Hutchisson(16) and later by Wagner (17), and Ansbacher (18). In general, such integrals are not easy to evaluate because $Q' \neq Q''$; in certain cases, however, and by using various approximations, overlap integrals of the type shown in eq. (3) can be quite easy to calculate. Smith and Warsop (19) have developed a method for calculating integrals of the type

$$R_{MO} = \int \psi_M' (Q') \, \psi_0'' (Q'') \, dQ' \qquad (4)$$

for large changes in shape. The integral shown in eq. (4) represents the overlap between the zero vibrational level of the lower electronic state with the vibrational level, M, in the upper electronic state.

To evaluate integrals of the type shown in eq. (4), one begins by relating the upper state normal coordinate Q' to the lower state normal coordinate Q" by the following relationship:

$$\underline{Q}' = \underline{A}\underline{Q}'' + \underline{d} \qquad (5)$$

where $\underline{A}$ is a square matrix which transforms the vector of ground state normal coordinates into the vector of upper state normal coordinates, and $\underline{d}$ is the change in the origin of the normal coordinates. Such a relationship is necessary so that $\underline{Q}'$ and $\underline{Q}''$ are functions of the same variable so that the integral over dQ' will have some meaning.

To simplify the relationship between $\underline{Q}'$ and $\underline{Q}''$, $\underline{A}$ is set to the unit matrix. Setting $\underline{A}$ equal to the unit matrix is rationalized by Coon, et. al. (20), who show that, for band progressions that originate in the v = 0 level of the ground electronic state, the vibrational wave function in the ground state is largely concentrated around the origin of the normal coordinate and thus

$$\underline{Q}'' \cong 0 \tag{6}$$

for a large percentage of the time. This can easily be seen if one graphs the harmonic oscillator wave functions for the v = 0 level. From this one can see that $\underline{Q}'$ will be very insensitive to $\underline{A}$ (since $\underline{Q}''$ is zero most of the time) but will be sensitive to $\underline{d}$. With $\underline{A}$ set to the unit matrix, eq. (5) becomes

$$\underline{Q}' = \underline{Q}'' + \underline{d} \tag{7}$$

and thus eq. (4) becomes

$$R_{MO} = \int \psi'(Q') \; \psi''(Q' - d) \, dQ' \tag{8}$$

Smith (21) has shown that for R_{MO} under the above conditions eq. (8) takes the form

$$R_{MO} = (2^{-M} \, q M!)^{1/2} \exp(1/4 \, \gamma^2 P) \sum_{\ell=o}^{M} \frac{(\gamma q)^{M-2t} \, (-X)^t}{(M - 2t)! \, t!}$$

where

$$q = \frac{2(\nu'\nu'')^{1/2}}{\nu''} \qquad p = \frac{\nu''\nu'}{\nu' + \nu''} \qquad \gamma = \alpha^{1/2} d$$

$$\alpha = \frac{4\pi^2 \nu c}{h} \qquad X = \frac{\nu'' - \nu'}{\nu'' + \nu'} \tag{9}$$

Thus, to carry out the calculation, all one needs to know are the lower and upper state frequencies and d_i, the shift in the origin of the normal coordinate being considered.

The vector of normal coordinates, $\underline{Q}$, is related to that of the internal symmetry coordinates by eq. (2). The vector of the shifts in the origins of the normal coordinates, $\underline{d}$, is related to $\Delta\underline{S}$, the vector of changes in the internal symmetry coordinates, in the same manner.

$$\underline{d} = \underline{L}^{-1} \quad \Delta\underline{S} \tag{10}$$

One should remember that in thionylimide, with the change in an internal symmetry coordinate being equal to the change in the corresponding internal coordinate, $\Delta\underline{S}$ represents directly the changes in bond angles and bond lengths between the upper and lower states.

To calculate $\underline{d}$ one must know the shape change occurring in the transition. In thionylimide, due to the diffuseness of the observed bands, no rotational analysis could be done and thus it was impossible to determine the structure of thionylimide in the excited state. Thus, to calculate $\underline{d}$, an appropriate excited state structure for thionylimide had to be assumed. The change of shape occurring in the 2900Å system of SO_2 was assumed to be the same as the shape change occurring in the 2700Å system of thionylimide. This is justified by the facts that the change of shape occurring in thionylimide is occurring on the SO end of the molecule, that both transitions have similar

vibrational structures, and that both transitions are the first strong transitions seen in each molecule.

In a preliminary band contour analysis of the (010)-(000) band [Metropolis's vibrational numbering (2)] of the 2900Å system of SO_2, Dixon (22) has found that in the excited state, $R_{SO} \tilde{=} 1.58$ Å and $\alpha_{OSO} = 105^o$. Since in the ground state $R_{SO} = 1.43$ Å and $\alpha_{OSO} = 119^o$ (22), $\Delta R_{SO} = 0.15$ Å and $\Delta\alpha_{OSO} = -15^o$ for the transition. Using these changes in bond lengths and bond angles and setting

$$\Delta R_{SO} = \Delta R_{NS} \tag{11}$$

one can calculate $\underline{d}$. Since the shape change has been reasoned to be taking place around the S atom, only the overlap integrals for ν_2, ν_3, and ν_5 [see table (2) for frequency assignments] need be considered since only these vibrations will have appreciable d_i's.

Using eqs. (10), and (11),

$$\underline{d} = \underline{L}''^{-1} \begin{bmatrix} \Delta R_{NH} \\ \Delta R_{NS} \\ \Delta R_{SO} \\ \Delta\alpha\,HNS \\ \Delta\alpha\,NSO \\ \Delta\gamma HNSO \end{bmatrix} = \underline{L}''^{-1} \begin{bmatrix} 0 \\ 0.15A \\ 0.15A \\ 0 \\ 0.26R \\ 0 \end{bmatrix} \tag{12}$$

Thus the individual d_i's of interest become

$$\begin{aligned} d_2 &= (1.936 - 1.995)(0.15) + (0.028)(0.26) = 0.052 \\ d_3 &= (1.923 + 2.596)(0.15) - (0.142)(0.26) = 0.674 \\ d_5 &= (1.067 + 0.874)(0.15) + (3.352)(0.26) = 1.163 \end{aligned} \tag{13}$$

From the above values of d_i for ν_2, ν_3, and ν_5, one can see that ν_3 and ν_5 will provide most of the intensity. One would therefore expect a long series of band progressions in both ν_3 and ν_5. The reason d_2 is small even though the vibration is centered on the S-O end of the molecule, is that it is mainly an asymmetric stretching vibration, thus the change in R_{NS} is counteracted by that in R_{SO}.

Since we cannot be sure of the vibrational analysis of the 2700Å system of thionylimide, the excited state frequencies cannot be determined unambiguously.

The NSO bending vibration, ν_5, was assumed to be 285 cm^{-1} (the predominant vibrational interval seen in the transition), by analogy with the 2900Å system of SO_2, where the upper state bending vibration (ν_2' = 318 cm^{-1}) is similarly prominent. This assignment is supported by the three previously mentioned "hot" bands which are all separated from bands known to be temperature-insensitive by the ground state frequency ν_5 = 453 cm^{-1} to within ± 25 cm^{-1} (i.e. for these diffuse bands within the accuracy of measurement). The other low-lying frequency, the torsional vibration ν_6'', at 759 cm^{-1}, cannot give rise to "hot" bands of this type because, since it is a non-totally symmetric vibration, it must obey the selection rule $\Delta v_6 = 0, \pm 2, \ldots$; then, "hot" bands arising from the level $v_6'' = 1$ are most likely to be sequence bands ($\Delta v=0$). However, the assignment of these "hot" bands as torsional sequence bands cannot

be entirely ruled out, though it is less likely than their assignment as the first members of ground state progressions in ν_5'', since these are favoured by the Boltzmann distribution law. ν_3 was estimated using the rule given by Birge (24) for diatomic molecules:

$$r^2\omega = \text{constant} \tag{14}$$

where r = internuclear distance and ω = vibration frequency. Thus:

$$r'^2\omega' = r''^2\omega''$$

$$\omega' = \left(\frac{r''}{r'}\right)^2\omega'' = 859 \text{ cm}^{-1} \tag{15}$$

A computer program written by Malm and Merer was used to evaluate eq. (9) using the previously determined d_i's and frequencies. The results of these calculations are given in Table (3) and are graphed in Fig. (11).

Upon examination of the spectrum of thionylimide taken on the Cary 14 spectrophotometer (fig. 6), one can see that the bands are not discernible along the whole transition, and one must consider the possibility that the absorption maximum and the banded structure may not correspond to the same excited state. The absorption maximum comes at approximately 2170Å (46083 cm^{-1}) and the first discernible band is at 2690Å (37175 cm^{-1}). If the observed absorption maximum and the banded structure are taken as arising from the same transition, the Franck-Condon maximum lies at least 8900 cm^{-1} from the system origin. The value shown in fig. (11) on the basis of Dixon's results for the 2900Å system of SO_2 is approximately 6000 cm^{-1}.

Thus the calculated transition is too "short" in relation to the observed transition provided the banded structure and the observed absorption maximum belong to the same transition.

Further calculations were done to correlate changes in ΔR_{NS} (= ΔR_{SO}) and $\Delta\alpha_{NSO}$ in the transition to the "length" of the transition (or the position of the Franck-Condon maximum); thus it was possible to see how large a shape change was necessary for the Franck-Condon maximum to lie 8900 cm^{-1} from the system origin. The results are shown in fig. (12). From fig. (12) one can see that to explain the value 8900 cm^{-1} in thionylimide, one needs ΔR_{NS} = 0.18Å and $\Delta\alpha_{NSO}$ = 0.28 Radian or other combinations from the graph. Thus one must accept approximately $R_{NS} \cong 1.69$Å, $R_{SO} \cong 1.63$ and $\alpha_{NSO} \cong 114^{o}$ in the excited state of thionylimide to explain the 2700Å system of thionylimide as a single transition. Such large changes in shape are approaching the limit for $\pi \rightarrow \pi^*$ transitions if one assumes one is seeing such a transition in thionylimide. The largest change of shape known for a $\pi \rightarrow \pi^*$ transition is in O_2 where there is a 33% change in the internuclear distance; thus in thionylimide where the π molecular orbital is spread over two bonds, one would expect that the maximum change in the NS or SO bond would be 16.5% which is 0.25Å in the NS bond and 0.24Å in the SO bond. These changes are not much larger than those listed above which are needed to explain the 2700Å system of thionlyimide as a single transition.

Table 2

Comparison of Reported Gas Phase Frequencies and Matrix Frequencies

	Richert (HNSO Q branches)	Matrix (HNSO)	Meaning
ν_1	3345 cm^{-1}	3309 cm^{-1}	ν_{NH}
ν_2	1261	1249	ν_{OSN} asym.
ν_3	1090	1083	ν_{OSN} sym.
ν_4	911	900	α_{NH}
ν_5	453	447	α_{NSO}
ν_6	755	754	γ_{HNSO}

	Richert's Force Constants	Author's Force Constants
f_{NS}	8.2 mdyne $\AA^{-1}$	7.48 mdyne $\AA^{-1}$
f_{SO}	8.6 "	8.4 "
f_{NH}		6.1 "
$f_{\alpha NSO}$	0.6 "	0.598 "
$f_{\alpha HNS}$		0.51 "
$f_{\gamma HNSO}$		0.22 "

Table 2 (continued)

Frequency fits for various isotopes using the force constants of this work

$HNS^{32}O$	OBS. FREQ. (cm^{-1})	CALC. FREQ. (cm^{-1})	DIFFERENCE (cm^{-1})	PERCENT ERROR
1	3309.0	3321.6	-12.6	-0.381
2	1249.0	1253.0	-4.0	-0.318
3	1083.0	1067.9	15.1	1.393
4	900.0	928.3	-28.3	-3.140
5	754.0	754.9	-0.9	-0.117
6	447.0	437.8	9.2	2.061

$HNS^{34}O$	OBS. FREQ. (cm^{-1})	CALC. FREQ. (cm^{-1})	DIFFERENCE (cm^{-1})	PERCENT ERROR
1	0.0	3321.6	0.0	0.0
2	1234.0	1239.3	-5.3	-0.429
3	0.0	1064.4	0.0	0.0
4	0.0	923.9	0.0	0.0
5	0.0	753.9	0.0	0.0
6	0.0	434.8	0.0	0.0

$DNS^{32}O$	OBS. FREQ. (cm^{-1})	CALC. FREQ. (cm^{-1})	DIFFERENCE (cm^{-1})	PERCENT ERROR
1	2450.0	2432.4	17.6	0.718
2	1245.0	1244.4	0.6	0.050
3	1048.0	1043.0	5.0	0.477
4	752.0	724.0	28.0	3.717
5	592.0	590.9	1.1	0.192
6	400.0	412.9	-12.9	-3.227

$DNS^{34}O$	OBS. FREQ. (cm^{-1})	CALC. FREQ. (cm^{-1})	DIFFERENCE (cm^{-1})	PERCENT ERROR
1	0.0	2432.4	0.0	0.0
2	1230.0	1230.0	-0.2	-0.018
3	0.0	1037.6	0.0	0.0
4	0.0	721.2	0.0	0.0
5	0.0	589.6	0.0	0.0
6	0.0	410.6	0.0	0.0

Table 2 (continued)

Eigenvector and Inverse Eigenvector Matrices for $HNS^{32}O$ Based on the Force Constants of this Work

EIGENVECTORS

FREQUENCY = 3321.9 cm^{-1}

1.0312 -0.0335 0.0005 -0.0429 0.0429 0.0

FREQUENCY = 1259.4 cm^{-1}

0.0082 0.2417 -0.2219 -0.4022 0.0202 0.0

FREQUENCY = 1075.3 cm^{-1}

0.0062 0.1750 0.2104 -0.3769 -0.0738 0.0

FREQUENCY = 932.7 cm^{-1}

0.0086 0.1102 0.0079 0.8863 -0.1230 0.0

FREQUENCY = 746.6 cm^{-1}

0.0 0.0 0.0 0.0 0.0 1.2215

FREQUENCY = 433.7 cm^{-1}

-0.0017 0.0158 0.0115 0.0707 0.2834 0.0

EIGENVECTOR INVERSE

FREQUENCY = 3321.9 cm^{-1}

0.9680 -0.0386 0.0006 -0.0034 0.0086 0.0

FREQUENCY = 1259.4 cm^{-1}

0.0535 1.9358 -1.9954 -0.2196 0.0284 0.0

FREQUENCY = 1075.3 cm^{-1}

0.0555 1.9230 2.5959 -0.2824 -0.1420 0.0

FREQUENCY = 932.7 cm^{-1}

0.1021 1.6093 0.1288 0.8824 -0.3144 0.0

Table 2 (continued)

FREQUENCY = 746.6 cm^{-1}

0.0	0.0	0.0	0.0	0.0	0.8187

FREQUENCY = 433.7 cm^{-1}

-0.0916	1.0666	0.8740	0.3255	3.3521	0.0

Table 3

Calculated values of R_{MN} for ν_3 and ν_5 with $R_{SO} = 0.15\text{Å}$ and $\Delta\alpha_{NSO} = 0.26$ Radian

ν_3		ν_5	
UPPER STATE FREQUENCY =	859.00 cm^{-1}	UPPER STATE FREQUENCY =	285.00 cm^{-1}
LOWER STATE FREQUENCY =	1050.00 cm^{-1}	LOWER STATE FREQUENCY =	450.00 cm^{-1}

v'	v" = 0	v'	v" = 0
0	0.055549	0	0.036467
1	0.140021	1	0.103645
2	0.245643	2	0.202506
3	0.346050	3	0.313296
4	0.414857	4	0.405846
5	0.436694	5	0.452940
6	0.411496	6	0.442376
7	0.351593	7	0.381074
8	0.274826	8	0.290026
9	0.197751	9	0.194110
10	0.131543	10	0.112692

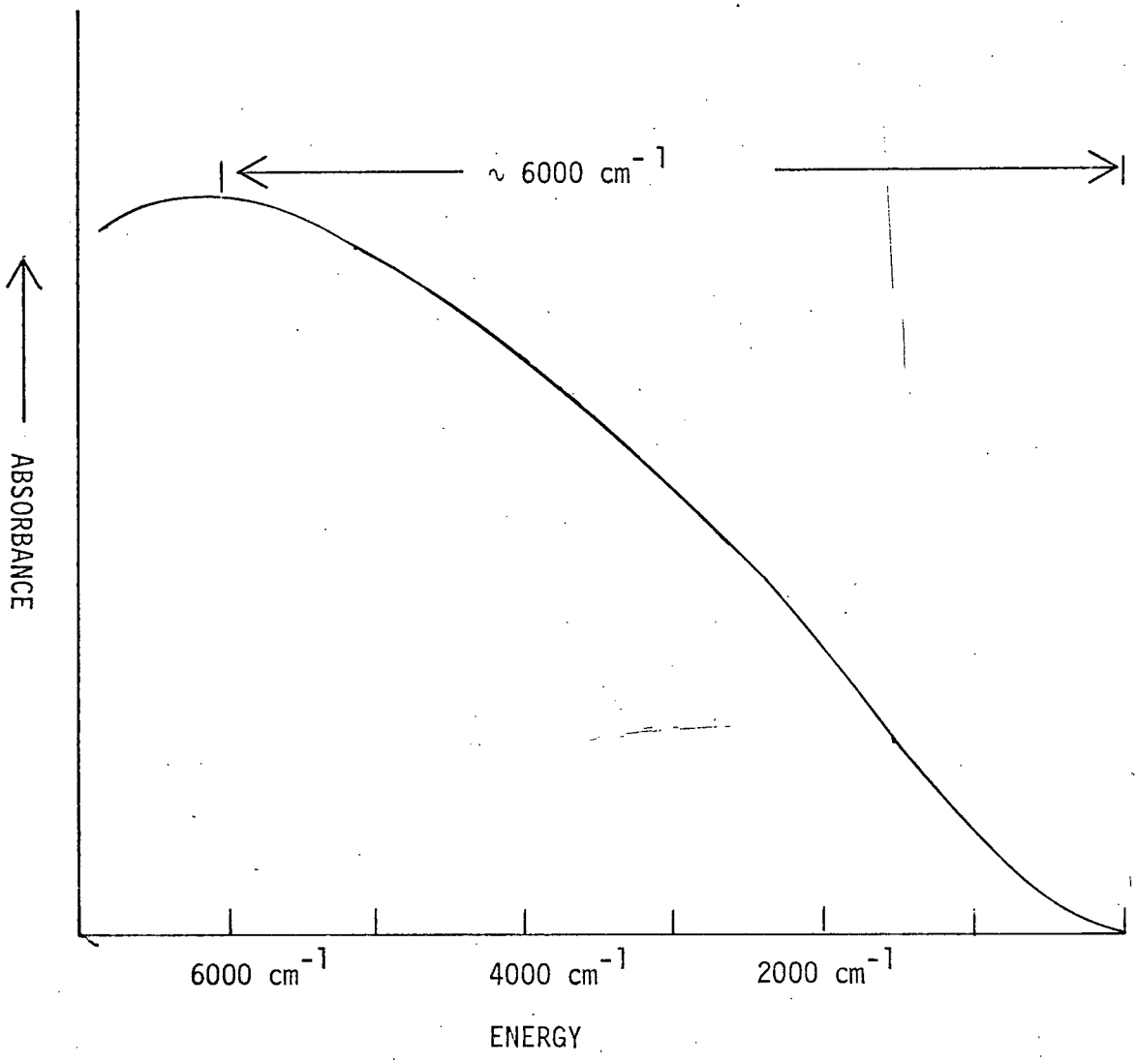

Fig. 11 Calculated transition envelope, for $\Delta R_{NS} = \Delta R_{SO} = 0.15$ Å and $\Delta\alpha_{NSO} = 15^{o}$

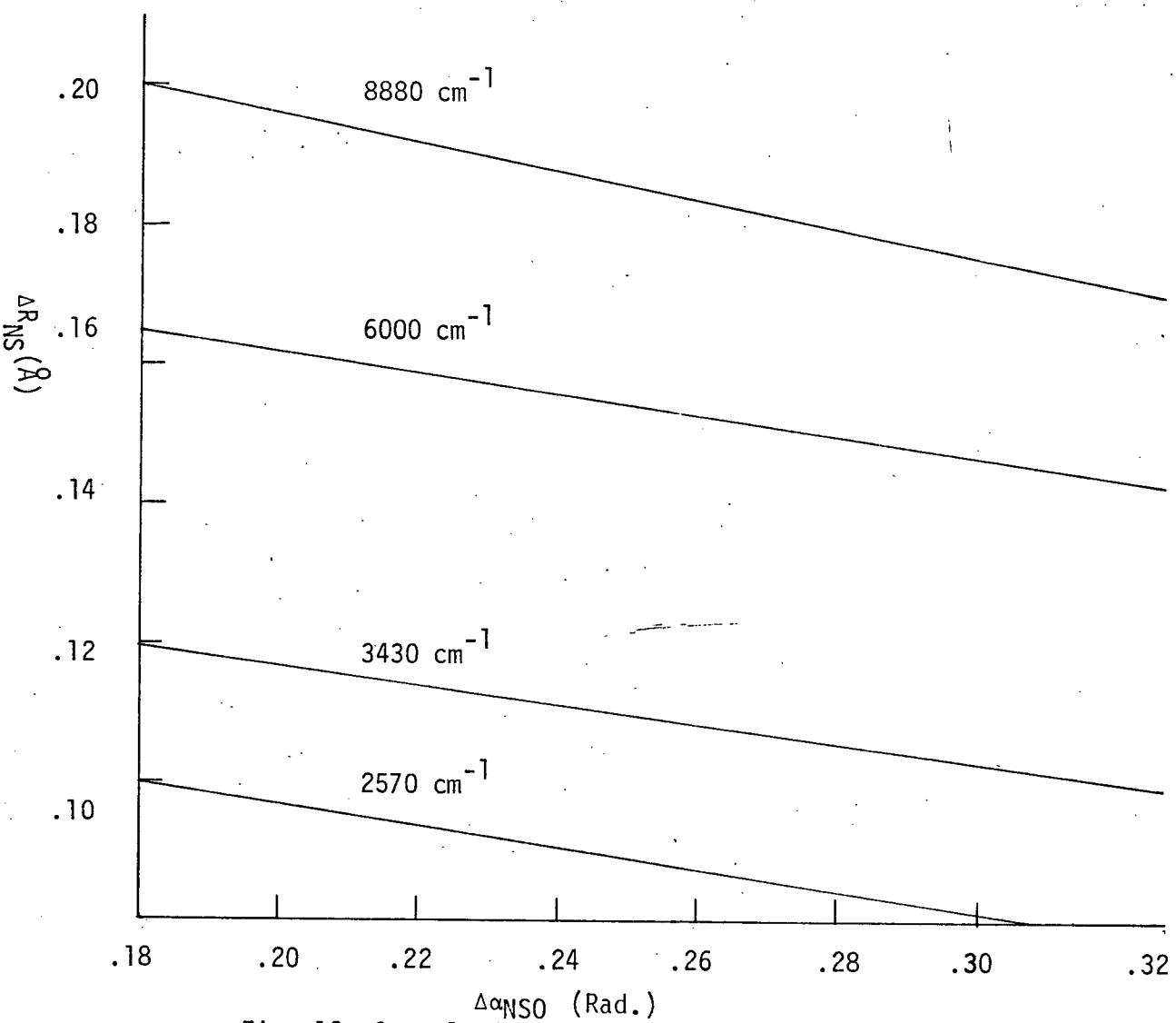

Fig. 12 Correlation of ΔR_{NS} and $\Delta\alpha_{NSO}$ with different system origin-absorption maximum separations

C. Electronic States of Thionylimide

To achieve an understanding of the absorption spectrum of HNSO, it is necessary to establish the possible electronic states of HNSO. There are two possible ways to proceed: either the electronic states of HNSO can be correlated with the states of the isoelectronic molecule, SO_2, or the electronic states of HNSO can be derived from a reasonable set of dissociation products. These two methods will each be considered.

States of HNSO derived from dissociation products

The most probable dissociation products will result from the rupture of the weakest bond in the molecule. Some relevant dissociation energies are given below (23).

$$SO_{2(g)} \rightarrow SO_{(g)} + O_{(g)} \qquad \Delta H = 5.9 \text{ e.v.}$$

$$NS_{(g)} \rightarrow N_{(g)} + S_{(g)} \qquad \Delta H = 5.61 \text{ e.v.}$$

$$HNO_{(g)} \rightarrow H_{(g)} + NO_{(g)} \qquad \Delta H = 2.11 \text{ e.v.}$$

$$NH_{3(g)} \rightarrow H_{(g)} + NH_{2(g)} \qquad \Delta H = 4.3 \text{ e.v.}$$

Although the bond energy of the NS radical is certainly greater than that in HNSO, it is reasonable to expect the N-H bond to be the weakest in the molecule. Thus the most likely dissociation process is

$$HNSO_{(g)} \rightarrow H_{(g)} + NSO_{(g)}$$

The ground state of HNSO will be formed from the dissociation products in their ground states. The H atom will be in the $1s^1\ ^2S$

atomic ground state. The nature of the ground state of NSO is more difficult to determine. NSO is isoelectronic with NO_2 and will probably have corresponding electron configurations and states. It is noted that NO_2 belongs to the C_{2v} point group, whereas NSO belongs to the C_s point group. (See Table(4)for C_{2v} and C_s character tables and the correlation of the irreducible representations of the C_{2v} and C_s point groups.)

NO_2 in its ground state has the following electron configuration (3):

$$(5a_1)^2\ (1a_2)^2\ (4b_2)^2\ (6a_1)\ \ldots\ {}^2A_1\ (C_{2v}),\ {}^2A'\ (C_s)$$

Here the numbers (5,1,4,6) refer to the number of times a certain representation has appeared in the molecular orbital configuration. Thus $5a_1$ refers to the fifth a_1 molecular orbital. One can see that the NSO radical in its ground state will probably be in a $^2A'$ state. Thus the ground state of HNSO will be formed from a (^2S) H atom and a ($^2A'$) NSO radical. Using the building up principles (23) one obtains $^{1,3}A'$ states of HNSO. It is seen that, for molecules with even numbers of electrons, no partially filled degenerate orbitals, or any near lying unfilled orbitals, Hund's Rule (23) does not hold and the singlet has the lower energy. Thus, according to this approach the ground state of HNSO will be the singlet and the triplet will be the first excited state.

The first excited state of NO_2 has the following electron configuration (23):

$$(5a_1)^2\ (1a_2)^2\ (4b_2)^2(2b_1)\ \ldots\ {}^2B_1\ (C_{2v}),\ {}^2A''\ (C_s)$$

Thus the first excited state of NSO will be a $^2A''$ state. From a (^2S) H atom and a ($^2A''$) NSO radical one obtains ($^{1,3}A''$) HNSO. As we shall see, the triplet will have the lower energy, and the singlet will have the higher energy. A potential energy diagram based on these results is shown in fig. (13).

Correlation of the Electronic States of SO_2 and HNSO

SO_2 has the following ground state and low-lying excited state electron configurations (23).

$$\ldots (1a_2)^2(4b_2)^2(6a_1)^2, \quad {}^1A_1 \quad \text{(ground state)}$$
$$\ldots (1a_2)^2(4b_2)^2(6a_1)^1(2b_1)^1, \quad {}^{1,3}B_1$$
$$\ldots (1a_2)^2(4b_2)^1(6a_1)^2(2b_1)^1, \quad {}^{1,3}A_2$$
$$\ldots (1a_2)^1(4b_2)^2(6a_1)^2(2b_1)^1, \quad {}^{1,3}B_2$$

The first excited state of SO_2, giving rise to the transition at 3900Å, has been identified as a $^3B_1$ state (25). Evidence obtained by Hochstrasser and Marchetti (26) from matrix isolation studies shows another triplet state lying close to the $^3B_1$ state, which is probably the $^3A_2$ state. The 2900Å system of SO_2, though much stronger than the 3900Å system of SO_2, is not as strong as would be expected for an allowed singlet transition. Dixon (22) has suggested that it may be a $^1A_2 - {}^1A_1$ vibronic-allowed transition where the $^1A_2$ state is interacting via the b_2 antisymmetric stretching vibration with a higher B_1 electronic state to give $^1B_1 - {}^1A_1$ vibronic bands.

On the basis of these results the following energy level diagram for SO_2 is drawn.

29622 cm^{-1}	$^1A_2$
~ 27000 cm^{-1}	$^3A_2$
25767 cm^{-1}	$^3B_1$
0 cm^{-1}	$^1A_1$

Using the correlation table for C_{2v} and C_s point groups, the lowest four states in HNSO are predicted to be $^1A'$, $^3A''$, $^3A''$, and $^1A''$ by correlation with the known states of SO_2. This method gives the same results as the previous method except that the first triplet is $^3A''$ instead of $^3A'$.

This discussion shows that the ground state of thionylimide is most likely to be a $^1A'$ electronic state. The first two excited electronic states are given as triplets by both methods. As noted in the experimental section, approximately 0.40 meter-atm. were necessary to observe the weak continuum in the 3440Å region. Such weak transitions are usually associated with spin forbidden transitions. The second triplet which is not observed may lie close to the first triplet or under the 2900Å system of SO_2, in either case being undetectable. The 2700Å system of thionylimide is probably the first singlet transition.

Diffuse bands are usually associated with predissociation. Predissociation occurs when an electronic state with discrete

energy levels has the same energy as an unbound or repulsive electronic state. Thus $^3A'$ shown in fig. (13) may be predissociating the $^1A''$ upper state of the 2700Å system. One should note that, as predissociation gets stronger, the diffuse vibrational bands themselves may no longer be discernible above the background. It is therefore possible that the observed Franck-Condon Maximum and the banded structure can be from the same excited electronic state given the acceptance of the large shape change proposed in Section B.

Table 4

Character Tables for the Point Groups C_s and C_{2v}

C_s	E	$\sigma_v(yz)$		
A'	1	1	y,z	R_x
A"	1	-1	x	R_y,R_z

C_{2v}	E	C_2	$\sigma_v(xy)$	$\sigma_v(yz)$		
A_1	1	1	1	1	z	
A_2	1	1	-1	-1		R_z
B_1	1	-1	1	-1	x	R_y
B_2	1	-1	-1	1	y	R_z

Correlation of the Irreducible Representations of the C_s and C_{2v} Point Groups

C_{2v}	C_s
A_1, B_2	A'
A_2, B_1	A"

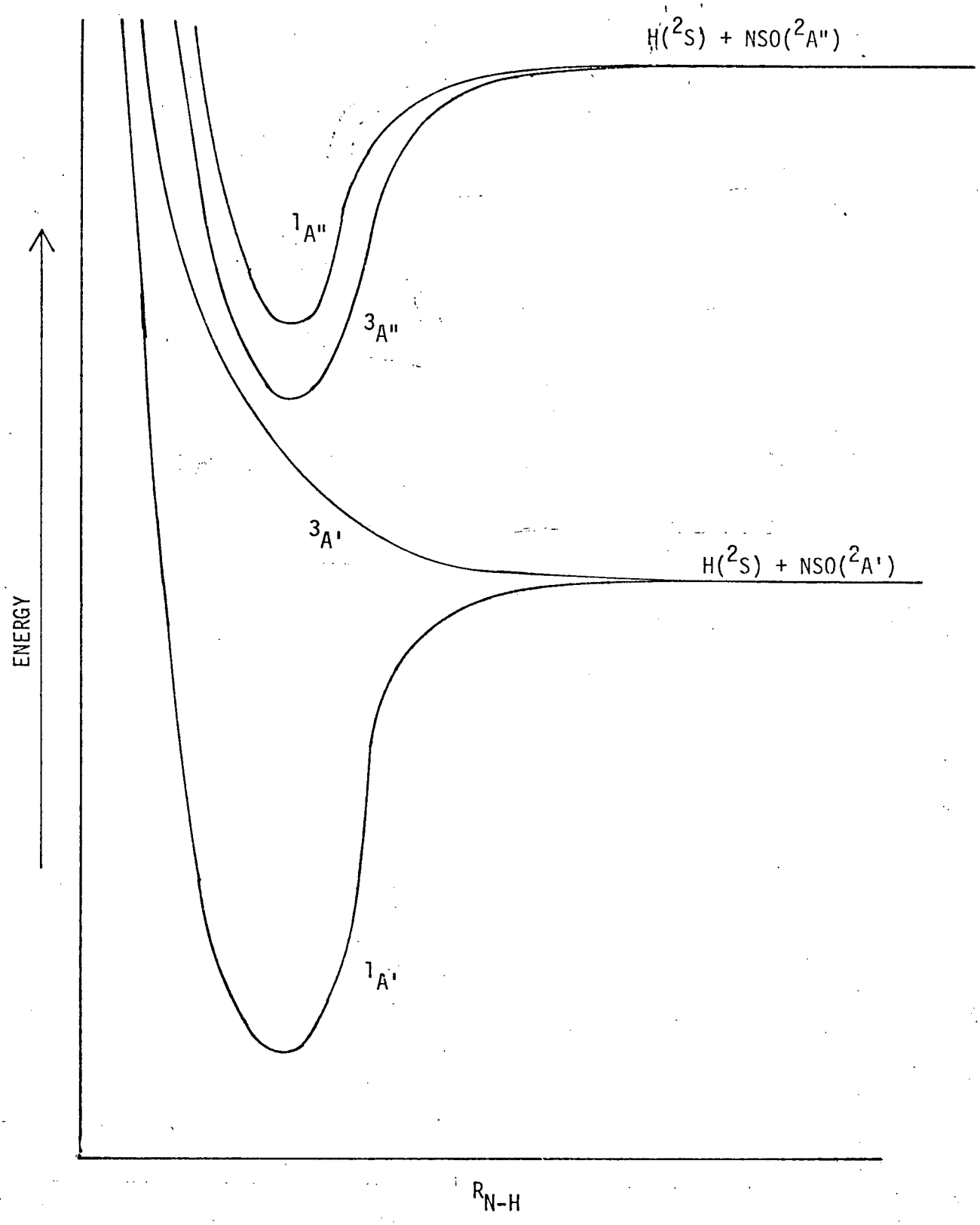

Fig. (13) Possible Potential Energy Curves for Thionylimide

CHAPTER II

$^2\Sigma$ and $^3\Sigma$ Electronic States of Linear Molecules in which One or More Quanta of a Degenerate Bending Vibration is Excited

2-1 Derivation of the Hamiltonian and its Matrix Elements

For a linear polyatomic molecule in a Σ electronic state, one normally assumes that the molecule is better described by Hund's Case (b) coupling where the spin is almost "free", being only coupled to the rotation of the molecule, due to the absence of any interaction coupling the spin to the axis of the molecule such as spin orbit coupling. In a Σ electronic state, a Hund's Case (a) representation, where the spin and vibrational angular momenta have well defined components along the axis of the molecule, is a good approximation as long as the molecule is not rotating or in low rotational quantum levels. At high rotational quantum numbers, a Hund's Case (b) representation is a better description, and the results obtained using a Case (a) hamiltonian will be transformed into Case (b) notation as needed.

The hamiltonian for a linear polyatomic molecule in a multiplet Σ electronic state in which one or more quanta of the degenerate bending vibration is excited is given below, following Van Vleck (27) and Watson (28).

$$H = B(r)\,[J_x - S_x - G_x)^2 + (J_y - S_y - G_y)^2] + 2\lambda(S_z^2 - \tfrac{1}{3}S^2) + \gamma(S_z^2 - S^2 + J_x S_x + J_y S_y) + \gamma'(G_z S_z) \qquad (1)$$

The first term is the ordinary rotational energy and involves only the x and y components since the rotational angular momentum vector is perpendicular to the molecular axis, which is taken as the z axis. In eq. (1), $J_{(x,y)}$, $S_{(x,y)}$, and $G_{(x,y)}$ are just the components of the total, the spin, and the vibrational angular momentum. The second term is the dipole-dipole spin-spin interaction, where λ is the spin-spin interaction constant. The third term is the spin-rotation interaction. The last term is a quasi spin-rotation interaction where the rotational motion arises from a degenerate bending vibration. This has been discussed by Chang and Chiu (29), but has not yet been seen experimentally.

Eq. (1) can be rewritten by first expanding and substituting with the following relationships:

$$\underset{\sim}{J}^2 - J_z^2 = J_x^2 + J_y^2 \qquad \text{and} \qquad \underset{\sim}{S}^2 - S_z^2 = S_x^2 + S_y^2 \qquad (2)$$

$$J \pm = J_x \pm i\, J_y \qquad\qquad S\pm = S_x \pm i\, S_y$$

Thus eq. (1) becomes

$$\begin{aligned} H = {} & B(r)[\underset{\sim}{J}^2 - J_z^2 + \underset{\sim}{S}^2 - S_z^2] + S_z^2(2\lambda+\gamma) \\ & - \underset{\sim}{S}^2(\gamma+\tfrac{2}{3}\lambda) + \gamma' G_z S_z + (\tfrac{1}{2}\gamma - B)(J_+ S_- + J_- S_+) - \\ & B(J_+ G_- + J_- G_+) + B(S_+ G_- + S_- G_+) + B(G_x^2 + G_y^2) \end{aligned} \qquad (3)$$

We now have the hamiltonian in a form in which we can discuss its matrix elements. The matrix elements of $\underset{\sim}{J}$ and $\underset{\sim}{S}$ are well known [see Van Vleck (27) and Hougen (30)] and are given below:

$$\begin{aligned}
\underset{\sim}{J}^2|J,P> &= J(J+1)\,\hbar^2|J,P> \\
\underset{\sim}{S}^2|S,\Sigma> &= S(S+1)\,\hbar^2|S,\Sigma> \\
J_z|J,P> &= P\hbar|J,P> \\
S_z|S,\Sigma> &= \Sigma\hbar|S,\Sigma> \\
J_{\mp}|J,P> &= [J(J+1)-P(P\pm1)]^{1/2}\ \hbar|J,P\pm1> \\
S_{\pm}|S,\Sigma> &= [S(S+1)-\Sigma(\Sigma\pm1)]^{1/2}\ \hbar|S,\Sigma\pm1>
\end{aligned} \tag{4}$$

Here P is the eigenvalue of the operator J_z. P is equal to $(\ell+\Sigma)$, where ℓ is the vibrational angular momentum quantum number, i.e. the eigenvalue of G_z, and Σ is the eigenvalue of S_z. $\underset{\sim}{S}$ has the normal sign of i in its commutation relationships but $\underset{\sim}{J}$ does not. This anomalous sign of i comes from the fact that, although $\underset{\sim}{J}$ has the normal sign of i in its commutation relationships when $\underset{\sim}{J}$ is referred to a space fixed axis system, when $\underset{\sim}{J}$ is referred to the molecule fixed axis system the anomalous sign of i appears in the commutation relationships for $\underset{\sim}{J}$. The sign change comes from the direction cosines which are used to transform the space fixed axes to the molecule fixed axes.

The matrix elements of $G_{\pm}$ are more complex. To obtain them, one starts with the definition of the Cartesian component G_α, $(\alpha=x,y,z)$

$$G_\alpha = \underline{Q}^{tr}\ \underline{\zeta}^{\alpha}\underline{P} \tag{5}$$

which relates G_α to the vector of the normal coordinates $\underline{Q}$ and their conjugate momenta $\underline{P}$. $\underline{\zeta}^\alpha$ is the Coriolis coupling coefficient matrix and is defined such that

$$(\underline{\zeta}^\alpha)_{uv} = (\underline{\ell}\,\underline{M}^\alpha\underline{\ell}^{tr})_{uv} \qquad \text{(u and v are vibrations)} \quad (6)$$

where $\underline{\ell}$ is the transformation matrix that transforms the mass weighted Cartesian displacement coordinates, $\underline{q}$, to normal coordinates, $\underline{Q}$.

$$\underline{Q} = \underline{\ell}\,\underline{q} \qquad (7)$$

$\underline{M}^\alpha$ is one of Meal and Polo's cross product matrices [see Meal and Polo (31)]. One should note that $\underline{\zeta}^\alpha$ is an antisymmetric matrix and therefore $\zeta^\alpha{}_{uv} = -\zeta^\alpha{}_{vu}$.

Most of the ζ coefficients are zero for linear molecules. The coefficient ζ_{uv} is only non-zero when the direct product of the irreducible representations of the vibrations u and v transforms as a rotation in the point group to which the molecule belongs. Thus in a symmetric triatomic linear molecule, only the σ_u^+ and π_u vibrations will have non-zero Coriolis coupling coefficients between them. Therefore only ζ_{23} (ζ_{32}) will be non-zero because $\Gamma_{v_2} \times \Gamma_{v_3} = \pi_u \times \sigma_u^+ = \pi_g$ where π_g is the species of the rotations R_x and R_y in the $D_{\infty h}$ point group. For an unsymmetrical triatomic molecule only $\zeta^\alpha{}_{21}$, $\zeta^\alpha{}_{12}$, $\zeta^\alpha{}_{32}$, and $\zeta^\alpha{}_{23}$ will be non-zero. For large molecules, the expression for G_α will become unwieldy. This thesis will therefore be restricted to unsymmetrical triatomic

molecules, but the formulae derived can be generalized for larger molecules. Eq. (5) for unsymmetrical triatomic molecules becomes

$$G_\alpha = \sum_{k=1,3} (Q_2 \zeta^\alpha_{2k} P_k + Q_k \zeta^\alpha_{k2} P_2) \tag{8}$$

Now defining $G_\pm$ as

$$G_\pm = G_x \pm i\, G_y \tag{9}$$

eq. (5) gives

$$G_\pm = \sum_{k=1,3} (\pm i\, Q_k \zeta^\alpha_{k2} P_{2\pm} \pm i\, Q_{2\pm} \zeta^\alpha_{2k} P_k); \alpha = (x,y) \tag{10}$$

and finally

$$G_\pm = \sum_{k=1,3} \zeta^\alpha_{2k} [\pm i\, Q_k P_{2\pm} \mp i\, P_k Q_{2\pm}] \tag{11}$$

The matrix elements of Q_k and P_k for a harmonic oscillator are given by Wilson, Decius, and Cross (32) and are

$$\begin{aligned}
\langle v_k + 1|P_k|v_k\rangle &= i\sqrt{\tfrac{1}{2}\hbar\nu_k(v_k+1)} \\
\langle v_k|P_k|v_k + 1\rangle &= -i\sqrt{\tfrac{1}{2}\hbar\nu_k(v_k+1)} \\
\langle v_k+1|Q_k|v_k\rangle &= \sqrt{\frac{h}{8\pi^2}\frac{1}{\nu_k}(v_k+1)} \\
\langle v_k|Q_k|v_k+1\rangle &= \sqrt{\frac{h}{8\pi^2}\frac{1}{\nu_k}(v_k+1)}
\end{aligned} \tag{12}$$

The matrix elements of $i\, P_{2\pm} \mp Q_{2\pm}$ for the doubly degenerate harmonic oscillator are given by Moffitt and Liehr (33), but will be given here in a slightly more useful form.

$$\langle v_2 \pm 1, \ell+1 | P_+ | v_2 \ell \rangle = \pm i[\tfrac{1}{2}h\nu_2]^{\frac{1}{2}}[(v_2+1)\pm(\ell+1)]^{\frac{1}{2}}$$

$$\langle v_2 \pm 1, \ell-1 | P_- | v_2 \ell \rangle = \pm i[\tfrac{1}{2}h\nu_2]^{\frac{1}{2}}[(v_2+1)\mp(\ell-1)]^{\frac{1}{2}}$$

$$\langle v_2 \pm 1, \ell+1 | Q_+ | v_2 \ell \rangle = [\frac{h}{8\pi^2\nu_2}]^{\frac{1}{2}}[(v_2+1)\pm(\ell+1)]^{\frac{1}{2}}$$

$$\langle v_2 \pm 1, \ell-1 | Q_- | v_2 \ell \rangle = [\frac{h}{8\pi^2\nu_2}]^{\frac{1}{2}}[(v_2+1)\mp(\ell-1)]^{\frac{1}{2}} \qquad (13)$$

Now it can be seen that for G_- and G_+ there will be four types of non-zero matrix elements for each.

$$\langle v_2 + 1, \ell\pm1, v_k+1 | G_\pm | v_2 \ell v_k \rangle = \mp \hbar\zeta_{2k}\Phi_k[(v_k+1)(v_2{}^{\pm\ell+2})]^{\frac{1}{2}}$$

$$\langle v_2 - 1, \ell\pm1, v_k+1 | G_\pm | v_2 \ell v_k \rangle = \pm \hbar\zeta_{2k}\Omega_k[(v_k+1)(v_2{}^{\mp\ell})]^{\frac{1}{2}}$$

$$\langle v_2 + 1, \ell\pm1, v_k-1 | G_\pm | v_2 \ell v_k \rangle = \mp \hbar\zeta_{2k}\Omega_k[v_k(v_2{}^{\pm\ell+2})]^{\frac{1}{2}} \qquad (14)$$

$$\langle v_2 - 1, \ell\pm1, v_k-1 | G_\pm | v_2 \ell v_k \rangle = \pm \hbar\zeta_{2k}\Phi_k[v_k(v_2{}^{\mp\ell})]^{\frac{1}{2}}$$

where k = 1,3 and, following Mills (34), with the definitions

$$\Omega_k = \tfrac{1}{2}\left[\sqrt{\frac{\nu_2}{\nu_k}} + \sqrt{\frac{\nu_k}{\nu_2}}\right]; \quad \Phi_k = \tfrac{1}{2}\left[\sqrt{\frac{\nu_2}{\nu_k}} - \sqrt{\frac{\nu_k}{\nu_2}}\right] \qquad (15)$$

Before beginning to evaluate the energy levels of the hamiltonian given in eq. (3), a suitable notation for the basis functions must be specified. Since the hamiltonian is set up in a Case (a) representation, where, as noted previously, the spin and vibrational angular momenta have well defined components along the molecular axis, a basis denoted by $\langle v_2, \ell, v_k, J, P, \Sigma |$ will be used. The symbols are as previously defined.

In eq. (3) the first four terms are diagonal in all quantum numbers. The last term $G_x^2 + G_y^2$, as shown by Hougen (35), only contributes small amounts to the anharmonicity constants x_{12}, x_{23}, and will be neglected. The fifth term which represents the spin-rotation interaction, is off-diagonal in Σ but diagonal in the vibrational quantum numbers. The sixth term involves $G_{\pm}$ and is therefore off-diagonal in the vibrational quantum numbers. It is this term which is responsible for the Coriolis interaction which resolves the degeneracy of states differing only in the sign of ℓ and brings about the familiar ℓ-type doubling. The seventh term is also off-diagonal in the vibrational quantum numbers and represents a "gyroscopic" spin-vibration interaction.

Since we are interested in the rotational energy levels in a given vibrational level, the elements off-diagonal in the vibrational quantum numbers must be taken into account correctly. This has been accomplished by the use of the Van Vleck transformation [Kemble (36)]

$$\langle v\ell'|\tilde{H}|v'\ell''\rangle = \sum_{v'\neq v} \frac{\langle v'\ell'|H|v\ell'''\rangle\langle v\ell'''|H|v'\ell''\rangle}{E_v - E_{v'}} \qquad (16)$$

For the case $v_2=v_k=\ell=0$ in a triplet state, the application of the Van Vleck transformation can be easily demonstrated. The $v_2=v_k=\ell=0$ level will only interact with the $v_2=v_k=1$, $\ell=\pm 1$ levels via the sixth and seventh terms. Shown in Table(5)are the matrix elements of these two terms. Upon application of the Van Vleck transformation, one obtains the second order correction to the

matrix for the $v_2=v_k=\ell=0$ vibrational level. The result is shown below.

	$\langle 0\ 0\ 0\ J\text{-}1\text{-}1\|$	$\langle 0\ 0\ 0\ J\ 0\ 0\|$	$\langle 0\ 0\ 0\ J\ 1\ 1\|$
$\langle 0\ 0\ 0\ J\text{-}1\text{-}1\|$	$\overline{B}^2[4J(J+1)]$	$-4\overline{B}^2\sqrt{2J(J+1)}$	0
$\langle 0\ 0\ 0\ J\ 0\ 0\|$		$\overline{B}^2[4J(J+1)+8]$	$-4\overline{B}^2\sqrt{2J(J+1)}$
$\langle 0\ 0\ 0\ J\ 1\ 1\|$	symmetric		$\overline{B}^2[4J(J+1)]$

$$\left(\overline{B}^2=\frac{-B^2\zeta^2\Phi^2}{\omega_k+\omega_2}\right) \qquad (17)$$

One can see that carrying out the Van Vleck transformation for higher vibrational levels will be very tedious. To avoid this procedure the results of carrying out the Van Vleck transformation in the general case were investigated, and the general forms of the resultant terms are tabulated in Table(6). The matrix elements of these operators can be evaluated using eqs. (4,14) and are given in Table(7)in terms of q, the normal ℓ-type doubling parameter for singlet states; $\tilde{\alpha}$, the Coriolis contribution to the effective B value for a given vibrational level; and $\tilde{g}$, the Coriolis contribution to g_{22}, the anharmonicity constant from the standard vibrational energy formula

$$E(v_2,\ell) = \omega_2(v_2 + 1) + g_{22}\ell^2 \qquad (18)$$

The matrix elements of the first three terms of the hamiltonian shown in eq. (3) are diagonal, and using eq. (4) are simply

$$\langle v_2\ell v_k JP\Sigma|H_{diag.}|v_2\ell v_k JP\Sigma\rangle = B[J(J+1)-(\ell+\Sigma)^2 + S(S+1)-\Sigma]^2 + \Sigma^2(2\lambda+\gamma)-S(S+1)(\gamma+\tfrac{2}{3}\lambda)+\gamma'\ell\Sigma \qquad (19)$$

The fifth term in eq. (3), the spin-rotation interaction, is off-diagonal in Σ, but is diagonal in v_2, ℓ, and v_k.

$$\langle v_2 \ell v_k JP, \Sigma \pm 1 | H_{J.S} | v_2 \ell v_k JP\Sigma \rangle =$$

$$(\tfrac{1}{2}\gamma - B)[J(J+1)-(\ell+\Sigma)(\ell+\Sigma\pm1)]^{\frac{1}{2}}[S(S+1)-\Sigma(\Sigma\pm1)]^{\frac{1}{2}} \qquad (20)$$

It is seen from eqs. (19,20) and Table(7)that it is possible to incorporate B and $\tilde{\alpha}_v$ into an effective B (B_v^{eff}) for a given vibrational level since the quantum number dependence of B and $\tilde{\alpha}_v$ are the same.

2-2 Results and Discussion

The results deal with both $^2\Sigma$ and $^3\Sigma$ electronic states in which v_2=1,2 and v_k=0, where v_2 corresponds to a degenerate bending vibration and v_k corresponds to a stretching vibration. These cases are the ones of prime interest because they are the cases most likely to be observed experimentally. Utilizing eqs. (19,20) and Table(7),the matrix correct to second order can be immediately written down in the Case (a) representation. Since all the resulting matrices are doubly symmetric, they can be factorized into smaller sub-matrices using the Wang transformation (37) [see Appendix 2]. These sub-matrices correspond to either the Kronig (+) or (-) rotational levels. The resulting sub-matrices can be diagonalized. The results can be transformed to a Case (b) representation as needed.

$^2\Sigma$ Electronic States

For the level $v_2=1$, $\ell=\pm1$, $v_k=0$, in a $^2\Sigma$ electronic state one obtains the matrix shown in Table (8) using eqs. (19,20) and Table (7). Use of the Wang transformation yields the following pair of matrices.

$\lvert\ell,\Sigma\rangle$	$\frac{1}{\sqrt{2}}\{\lvert 1,\frac{1}{2}\rangle \pm \lvert -1,-\frac{1}{2}\rangle\}$	$\frac{1}{\sqrt{2}}\{\lvert 1,-\frac{1}{2}\rangle \pm \lvert -1,\frac{1}{2}\rangle\}$
$\frac{1}{\sqrt{2}}\{\lvert 1,\frac{1}{2}\rangle \pm \lvert -1,-\frac{1}{2}\rangle\}$	$B_1[J(J+1)-\frac{7}{4}]$ $+\frac{1}{2}\gamma'-\frac{1}{4}\gamma$	$-(B_1-\frac{1}{2}\gamma)\sqrt{J(J+1)-\frac{3}{4}}$ $\pm\frac{1}{2}q_1\sqrt{[J(J+1)+\frac{1}{4}][J(J+1)-\frac{3}{4}]}$
$\frac{1}{\sqrt{2}}\{\lvert 1,-\frac{1}{2}\rangle \pm \lvert -1,\frac{1}{2}\rangle\}$	symmetric	$B_1[J(J+1)+\frac{1}{4}]-\frac{1}{4}\gamma$ $-\frac{1}{2}\gamma'\pm(-q_1)\sqrt{J(J+1)}$

(21)

These two matrices (differing in the sign of the q terms) can easily be diagonalized to give four energy levels. The general energy equation is given below.

$$E = B_1[(J+\tfrac{1}{2})^2-1]-\tfrac{1}{2}\gamma\mp\tfrac{1}{2}q(J+\tfrac{1}{2}) \pm$$

$$\{[\tfrac{1}{2}\gamma'-B_1\pm\tfrac{1}{2}q(J+\tfrac{1}{2})^2]^2+[\tfrac{1}{2}\gamma-B_1\pm\tfrac{1}{2}q(J+\tfrac{1}{2})^2]^2[(J+\tfrac{1}{2})^2-1]\}^{\frac{1}{2}} \qquad (22)$$

One should notice that in generating the four energy levels, one must be consistent in the choice of sign of the q terms, but this choice is independent of the sign of the square root. Since

the matrix can be diagonalized exactly, one just has to substitute ($N=J+\frac{1}{2}$) and ($N=J-\frac{1}{2}$) to obtain the results in Case (b) notation. Thus eq. (22) becomes

$$F_2(N=J+\tfrac{1}{2})=B_1(N^2-1)-\tfrac{1}{2}\gamma\mp\tfrac{1}{2}qN+\{[\tfrac{1}{2}\gamma'-B_1\pm\tfrac{1}{2}qN]^2 + [\tfrac{1}{2}\gamma-B_1\pm\tfrac{1}{2}qN]^2[N^2-1]\}^{\frac{1}{2}} \quad (23)$$

$$F_1(N=J-\tfrac{1}{2})=B_1(N^2+2N)-\tfrac{1}{2}\gamma\mp\tfrac{1}{2}q(N+1) - \{[\tfrac{1}{2}\gamma'-B_1\pm\tfrac{1}{2}q(N+1)]^2 + [\tfrac{1}{2}\gamma-B_1\pm\tfrac{1}{2}q(N+1)][N^2+2N]\}^{\frac{1}{2}} \quad (24)$$

The above equations correspond to the formulae that Hill and Van Vleck (27) have derived for $^2\Pi$ electronic states if the terms in γ and q are omitted, and γ' is substituted for the spin-orbit coupling constant, A. Thus one can see by analogy to $^2\Pi$ electronic states that, unless γ' is large, the splitting it will cause will be quenched by the spin uncoupling, and will merge into the spin-rotation interaction splitting as the molecule rotates faster and faster; that is, the effect of $\gamma' G_z S_z$ in coupling the spin to the molecular axis will be overcome by the term $-(B-\frac{1}{2}\gamma)(J_+S_- + J_-S_+)$. If γ' is negligible and B is large compared with γ, the terms under the square root sign in eqs. (23,24) can be simplified, and the equations reduce to the equations used for $^2\Pi$ vibronic levels of $^2\Sigma$ electronic states given by Johns (38), where the spin doubling and ℓ-type doubling are separate entities. These equations are given here.

$$F_2(N)=B[N(N+1)-1] - \tfrac{1}{2}\gamma(N+1) \pm \tfrac{1}{2}qN(N+1) \qquad (25)$$

$$F_1(N)=B[N(N+1)-1] + \tfrac{1}{2}\gamma(N) \pm \tfrac{1}{2}qN(N+1) \qquad (26)$$

Thus if γ' is negligible and $B_1 \pm \tfrac{1}{2}q(J+\tfrac{1}{2}) >> \gamma$, the spin splitting and ℓ-type doubling are indeed separate.

When two quanta of a degenerate bending vibration are excited, $^2\Sigma$ ($\ell=0$) and $^2\Delta$ ($\ell=\pm 2$) vibronic states are formed. Using eqs. (19,20) and Table(7),the corresponding matrix can be written down. Upon application of the Wang transformation one produces the two 3 x 3 matrices given in Table(9). To obtain the Case (b) representation, where the rotational energy is diagonal, it is necessary to find the matrix $\underline{S}$ such that

$$\underline{S}\,\underline{H}_{rot}(\text{case a})\,\underline{S}^{-1} = \underline{H}_{rot}(\text{case b}) \qquad (27)$$

To obtain the transformation matrix $\underline{S}$ for the $^2\Delta$ sub matrices one proceeds to set up the problem as follows. Written out in full eq. (27) becomes

$$\underline{S} \begin{bmatrix} B[(J+\frac{1}{2})^2-2] & -B\sqrt{(J+\frac{1}{2})^2-4} \\ -B\sqrt{(J+\frac{1}{2})^2-4} & B[(J+\frac{1}{2})^2-6] \end{bmatrix} \underline{S}^{-1} \qquad (28)$$

$$\begin{matrix} (N=J-\frac{1}{2}) & (N=J+\frac{1}{2}) \end{matrix}$$

$$= \begin{bmatrix} B[N(N+1)-4] & 0 \\ 0 & B[N(N+1)-4] \end{bmatrix}$$

The Case (b) matrix is in terms of N and not J. To write the Case (b) matrix in terms of J, one substitutes $N=J+\frac{1}{2}$ and $N=J-\frac{1}{2}$ respectively, for the two N values. The Case (b) matrix becomes

$$B\begin{bmatrix} J^2-\frac{17}{4} & 0 \\ 0 & J^2+2J-\frac{13}{4} \end{bmatrix}$$

Now, solving for the matrix $\underline{S}^{-1}$, one obtains for the lower eigenvalue, $B(J^2-\frac{17}{4})$, the following simultaneous equations

$$\begin{bmatrix} (J+\frac{1}{2})^2-2-J^2+\frac{17}{4} & -\sqrt{(J+\frac{1}{2})^2-4} \\ -\sqrt{(J+\frac{1}{2})^2-4} & (J+\frac{1}{2})^2-6-J^2+\frac{17}{4} \end{bmatrix} \begin{bmatrix} S_{12}^{-1} \\ S_{22}^{-1} \end{bmatrix}=0 \quad (29)$$

Therefore:

$$S_{22}^{-1} = \sqrt{\frac{J+\frac{5}{2}}{2(J+\frac{1}{2})}} \quad , \quad S_{12}^{-1} = \sqrt{\frac{J+\frac{3}{2}}{2(J+\frac{1}{2})}}$$

For the upper eigenvalue, $B(J^2+2J-\frac{13}{4})$ one similarly obtains

$$S_{21}^{-1} = \sqrt{\frac{J-\frac{3}{2}}{2(J+\frac{1}{2})}} \quad , \quad S_{11}^{-1} = \sqrt{\frac{J+\frac{5}{2}}{2(J+\frac{1}{2})}}$$

Thus

$$\underset{\sim}{S}^{-1} = \begin{bmatrix} \left[\frac{J+\frac{5}{2}}{2(J+\frac{1}{2})}\right]^{\frac{1}{2}} & -\left[\frac{J-\frac{3}{2}}{2(J+\frac{1}{2})}\right]^{\frac{1}{2}} \\ \left[\frac{J-\frac{3}{2}}{2(J+\frac{1}{2})}\right]^{\frac{1}{2}} & \left[\frac{J+\frac{5}{2}}{2(J+\frac{1}{2})}\right]^{\frac{1}{2}} \end{bmatrix} \tag{30}$$

Since the hamiltonian was set up in a molecule-fixed axis system, care must be taken with the phases of the results when applying them to a space fixed axis system due to the previously mentioned anomalous sign of i in the commutation relationships of J. This would be important in doing intensity calculations for the branches of a band involving such a state [see Hougen (39)].

Transforming the entire Case (a) matrix results in the Case (b) matrix shown in Table(9). The γ' terms have been omitted from the Case (b) matrix because they are likely to be negligible. There are terms off diagonal in γ in the Case (b) matrix that do not normally appear in the Case (b) formalism. These terms have been retained because the spin-rotation interaction in the Case (b) hamiltonian is usually written

$$H_{S\cdot R} = \gamma \underset{\sim}{N}\cdot\underset{\sim}{S} \tag{31}$$

This formalism is only good for Σ vibronic states, where N_z is zero, and in the above case N_z is definitely non-zero. This is discussed by Freed (40) and Carrington, et. al. (41).

$^3\Sigma$ Electronic States

The formulae for $^3\Sigma$ electronic states are of interest because data are available for the zero point levels of molecules in $^3\Sigma$ states (NCN, HCCN, C_2N_2), but as yet no bands involving degenerate vibrational levels have been analyzed. One can calculate energy level patterns for v_2=1,2 and determine what form the predicted energy level pattern will take. In triplet states there are effects from λ, the spin-spin interaction, which are not present in the doublet states. As in doublet states, the vibrational angular momentum will upset the normal spin splitting pattern until the rotation of the molecule quenches it by uncoupling it from the axis.

For the v_2=1 level (v_k=0) in a $^3\Sigma$ electronic state, one obtains from the Wang transformation two 3 x 3 matrices. These are shown in Table(10). To determine the corresponding Case (b) matrices one proceeds in the same manner as for the v_2=2 level in a $^2\Sigma$ electronic state. The result is given in Table(10) below the Case (a) matrices. For v_2=2 the Wang transformation yields a 4 x 4 and a 5 x 5 matrix, shown in Table(11). The (-) signs in the matrix correspond to the 4 x 4 matrix and the (+) signs to the 5 x 5 matrix. The 4 x 4 matrix is comprised of the three $^3\Delta$ states and the $^3\Sigma_1$ state. The very complicated Case (b) matrix is given below the Case (a) matrix.

A computer program written by Merer was used to diagonalize the Case (a) matrices for v_2=1,2 for the following cases of

interest: the $\tilde{a}\ ^3\Sigma_u^+$ state of C_2N_2 (42), the $\tilde{X}^3\Sigma_g^-$ state of NCN (43), and the $^3\Sigma$ states involved in the 3200Å transition of HCCN (4). There are published values for B, λ, and γ for the v=0 levels of C_2N_2 and NCN. There is no information for g, but q can be calculated. Data for HCCN are limited. The value $|\lambda| = 0.43\ cm^{-1}$ for the ground state of HCCN is obtainable from the ESR spectrum (44). The B value is approximately $0.36\ cm^{-1}$. If the spin-rotation constant is small (0.001), λ in the upper state is estimated as being $1.7\ cm^{-1}$ or $0.8\ cm^{-1}$, depending on the sign of λ in the ground state, from the observed head-head separations.

Figures (14 a,b,c) show the results of these calculations although no attempt is made to show ℓ-type doubling effects. The term $B[N(N+1)-\ell^2]$ has been substracted from the energy.

Examination of figs. (14 a,b,c) reveals that the $^3\Pi$ and $^3\Delta$ vibronic levels do not have the same form as the $^3\Sigma$ vibronic levels. It is also seen that, depending on the relative sizes of B, λ, and γ, there must be a convergence of $^3\Pi$, $^3\Delta$, and $^3\Sigma$ vibronic states at high N values. However, the normal $^3\Sigma$ energy levels are not conformed to at low N values. In C_2N_2 where λ and B are of the same order of magnitude and γ is large, the patterns for $^3\Delta$, $^3\Pi$, and $^3\Sigma$ converge very quickly and only for low values of N will any deviation from the normal $^3\Sigma$ pattern be seen. The opposite is observed in HCCN where there is quite a large deviation between $^3\Pi$, $^3\Delta$, and $^3\Sigma$ vibronic levels.

As mentioned previously, the ℓ-type doubling is not shown in figs. (14 a,b,c), although it was calculated for the v_4=1

level of HCCN. At high N values the normal ℓ-type doubling pattern for singlets is followed given by the equation

$$\Delta\nu = qN(N+1) \tag{32}$$

but at low N values the ℓ-type doubling pattern is erratic. With q set at 0.003 cm^{-1}, the theoretical ℓ-type doubling was calculated and plotted in fig. (15) with the deviation from eq. (32) as a function of N.

In the analysis of actual bands (yet to be done),it will be found that the normal $^3\Sigma$ combination relations,based on the formulae for $^3\Sigma$ levels given by Miller and Townes (45), used for evaluating the parameters λ and γ will break down as the rotational branches are followed back to the band origin. This can be illustrated by the following relationship,

$$F_1(N-1)-F_2(N-1)+F_3(N+1)-F_2(N+1)=-(2\lambda-\gamma) \tag{33}$$

where,as N decreases,the left hand side of the equation will become smaller than the right hand side. For N=10 in the $^3\Delta$ vibronic level of the given state of HCCN,the difference will be nearly 0.4 cm^{-1}. Also,the intensities will probably not follow the normal $^3\Sigma$ pattern and it may be necessary to examine the form of the intensities to analyze the bands.

TABLE 5

Elements off diagonal in the vibrational quantum numbers for the $v_2 = 0$ level in $^3\Sigma$ states

	|000J-1-1>	|000J00>	|000J11>
< 1,-1,0,J,-2,-1|	$-B\zeta\Phi\ \sqrt{2J(J+1)-4}$		
< 1,-1,0,J,-1,0|	$2B\zeta\Phi$	$-B\zeta\Phi\ \sqrt{2J(J+1)}$	
< 1,-1,0,J,0,1|		$2B\zeta\Phi$	$-B\zeta\Phi\ \sqrt{2J(J+1)}$
< 1,1,0,J,0,-1|	$B\zeta\Phi\ \sqrt{2J(J+1)}$	$-2B\zeta\Phi$	
< 1,1,0,J,1,0|		$B\zeta\Phi\ \sqrt{2J(J+1)}$	$-2B\zeta\Phi$
< 1,1,0,J,2,1|			$B\zeta\Phi\ \sqrt{2J(J+1)-4}$

Table 6 Effective Operators Arising from Second-Order Transformation of the Hamiltonian

Term	Selection Rules $\Delta\ell$	ΔP	$\Delta\Sigma$	Meaning
$B^2(J_+J_-G_-G_+ + J_-J_+G_+G_-)/\Delta\nu$	0	0	-	Diagonal α and g_{22} term
$B^2(S_+S_-G_-G_+ + S_-S_+G_+G_-)/\Delta\nu$	0	-	0	Diagonal α term resulting from spin
$-B^2(J_-S_+G_+G_- + J_+S_-G_-S_+)/\Delta\nu$	0	± 1	± 1	Vibrational γ term
$-B^2(J_+S_+G_-^2 + J_-S_-G_+^2)/\Delta\nu$	± 2	± 1	∓ 1	$\Delta P = \pm 1$ ℓ-type doubling all multiplicities
$B^2(J_+^2G_-^2 + J_-^2G_+^2)/\Delta\nu$	± 2	± 2	-	Normal ℓ-type doubling for singlets
$B^2(S_+^2G_-^2 + S_-^2G_+^2)/\Delta\nu$	± 2	-	∓ 2	"Diagonal" ℓ-type doubling for triplets

$\Delta\nu = (\omega_2 \pm \omega_k)$

Table 7 Matrix Elements of the Effective Operators Given in Table 6, in Harmonic Approximation

$$\langle v_2 J \ell\ \Sigma\ |\tilde{H}|\ v_2 J\ \ell\ \Sigma\rangle = \tilde{g}\ell^2 - \alpha_v[J(J+1)-(\ell+\Sigma)^2+S(S+1)-\Sigma^2]$$

$$\langle v_2 J \ell\ \Sigma\ |\tilde{H}|\ v_2 J\ \ell \pm 2\ \Sigma\rangle = \tfrac{1}{4}q\sqrt{(v_2 \mp \ell)(v_2 \pm \ell+2)}\sqrt{J(J+1)-(\ell+\Sigma)(\ell+\Sigma\pm1)}\sqrt{J(J+1)-(\ell+\Sigma\pm1)(\ell+\Sigma\pm2)}$$

$$\langle v_2 J \ell\ \Sigma \pm 2|\tilde{H}|\ v_2 J \ell \pm 2\ \Sigma\rangle = \tfrac{1}{4}q\sqrt{(v_2 \mp \ell)(v_2 \pm \ell+2)}\sqrt{S(S+1)-\Sigma(\Sigma\pm1)}\sqrt{S(S+1)-(\Sigma\pm1)(\Sigma\pm2)}$$

$$\langle v_2 J \ell\ \Sigma \pm 1|\tilde{H}|\ v_2 J \ell \pm 2\ \Sigma\rangle = -\tfrac{1}{2}q\sqrt{(v_2 \mp \ell)(v_2 \pm \ell+2)}\sqrt{J(J+1)-(\ell+\Sigma\pm1)(\ell+\Sigma\pm2)}\sqrt{S(S+1)-\Sigma(\Sigma\pm1)}$$

$$\langle v_2 J \ell\ \Sigma \pm 1|\tilde{H}|\ v_2 J \ell\ \Sigma\rangle = \tilde{\alpha}_v\sqrt{J(J+1)-(\ell+\Sigma)(\ell+\Sigma\pm1)}\sqrt{S(S+1)-\Sigma(\Sigma\pm1)}$$

where

$q = -4B_e^2 \sum_{k\neq 2}\left(\frac{\zeta_{2k}^2\Omega_k^2}{\omega_2-\omega_k} - \frac{\zeta_{2k}^2\Phi_k^2}{\omega_2+\omega_k}\right) = \frac{2B_e^2}{\omega_2}\left(1 + 4\sum_{k\neq 2}\frac{\zeta_{2k}^2\omega_2^2}{\omega_k^2-\omega_2^2}\right)$, i.e. such that ℓ-type doubling of the $v_2 = 1$ level of a $^1\Sigma$ electronic state is given by

$$\Delta\nu = qJ(J+1),$$

$\tilde{\alpha}_v = -2B_e^2 \sum_{k\neq 2}\left(\frac{\zeta_{2k}^2\Omega_k^2 v_2}{\omega_2-\omega_k} - \frac{\zeta_{2k}^2\Phi_k^2(v_2+2)}{\omega_2+\omega_k}\right)$ i.e. such that the effective B-value for the level v_2 is given by $(B_e - \tilde{\alpha}_v)$, and $\tilde{g} = 2B_e^2 \sum_{k\neq 2}\left(\frac{\zeta_{2k}^2\Omega_k^2}{\omega_2-\omega_2} + \frac{\zeta_{2k}^2\Phi_k^2}{\omega_2+\omega_k}\right)$. The quantity $\hbar^2$ has been suppressed here.

Table 8

Matrix for $v_2 = 1$ for $^2\Sigma$ Electronic States Correct to Second Order

$\lvert \ell\Sigma \rangle$	$\lvert 1,\frac{1}{2} \rangle$	$\lvert 1,-\frac{1}{2} \rangle$	$\lvert -1,\frac{1}{2} \rangle$	$\lvert -1,-\frac{1}{2} \rangle$
$\lvert 1,\frac{1}{2} \rangle$	$B_1[J(J+1)-\frac{7}{4}]+\frac{1}{2}\gamma'-\frac{1}{4}\gamma$	$-(B_1-\frac{1}{2}\gamma)\sqrt{J(J+1)-\frac{7}{4}}$	$\frac{1}{2}q_1\sqrt{[J(J+1)+\frac{1}{4}][J(J+1)-\frac{3}{4}]}$	(0)
$\lvert 1,-\frac{1}{2} \rangle$		$B_1[J(J+1)+\frac{1}{4}]-\frac{1}{4}\gamma$ $-\frac{1}{2}\gamma'$	$-q\sqrt{J(J+1)}$	$\frac{1}{2}q_1\sqrt{[J(J+1)+\frac{1}{4}][J(J+1)-\frac{3}{4}]}$
$\lvert -1,\frac{1}{2} \rangle$			$B_1[J(J+1)+\frac{1}{4}]$ $-\frac{1}{4}\gamma-\frac{1}{2}\gamma'$	$-(B_1-\frac{1}{2}\gamma)\sqrt{J(J+1)-\frac{7}{4}}$
$\lvert -1,-\frac{1}{2} \rangle$	Symmetric			$B_1[J(J+1)-\frac{7}{4}] + \frac{1}{2}\gamma' - \frac{1}{4}\gamma'$

Table 9 Matrices for $v_2=2$ in a $^2\Sigma$ Electronic State

Case (a) representation

	$\vert^2\Delta_{5/2}\rangle$	$\vert^2\Delta_{3/2}\rangle$	$\vert^2\Sigma_{1/2}\rangle$
$\langle^2\Delta\ \frac{5}{2}\vert$	$2\omega_2+4g_{22}+B_2[(J+\frac{1}{2})^2-6]-\frac{1}{2}\gamma+\gamma'$	$(\frac{1}{2}\gamma-B_2)[(J+\frac{1}{2})^2-4]^{\frac{1}{2}}$	$\frac{1}{2}q\{2[(J+\frac{1}{2})^2-1][(J+\frac{1}{2})^2-4]\}^{\frac{1}{2}}$
$\langle^2\Delta\ \frac{3}{2}\vert$		$2\omega_2+4g_{22}+B_2[(J+\frac{1}{2})^2-2]$ $-\frac{1}{2}\gamma-\gamma'$	$q\{2[(J+\frac{1}{2})^2-1]\}^{1/2}\{\pm\frac{1}{2}(J+\frac{1}{2})-1\}$
$\langle^2\Sigma\ \frac{1}{2}\vert$	symm		$2\omega_2\pm(\frac{1}{2}\gamma-B_2)(J+\frac{1}{2})+B_2(J+\frac{1}{2})^2-\frac{1}{2}\gamma$

The basis functions are the 'sum' functions of the Wang transformation for the upper signs in the third column, and 'difference' functions for the lower signs; thus if the plus signs are taken, the basis functions are of the type

$$^2\Delta_{5/2}\rangle = 2^{-\frac{1}{2}}\{\vert\ell=2,\ \Sigma=\tfrac{1}{2},J\rangle + \vert\ell=-2,\ \Sigma=-\tfrac{1}{2},\ J\rangle\}$$

For the $^2\Sigma$ vibronic state this implies the F_1 ($N=J-\frac{1}{2}$) rotational levels for the upper signs, and the F_2 ($N=J+\frac{1}{2}$) rotational levels for the lower signs.

Case (b) representation

	$\lvert^2\Delta(F_2)\rangle$	$\lvert^2\Delta(F_1)\rangle$	$\lvert^2\Sigma\rangle$
$\langle^2\Delta(F_2)\rvert$	$2\omega_2+4g_{22}+[B_2-\gamma/2(J+\frac{1}{2})][(J+\frac{1}{2})(J+\frac{3}{2})-4]$	$\gamma[(J-\frac{3}{2})(J+\frac{3}{2})]^{\frac{1}{2}}/(J+\frac{1}{2})$	Upper sign: 0 Lower sign: $-q[(J-\frac{1}{2})(J+\frac{1}{2})(J+\frac{3}{2})(J+\frac{5}{2})]^{\frac{1}{2}}$
			Upper sign: $q[(J-\frac{3}{2})(J-\frac{1}{2})(J+\frac{1}{2})(J+\frac{3}{2})]^{\frac{1}{2}}$
$\langle^2\Delta(F_1)\rvert$		$2\omega_2+4g_{22}+[B_2+\gamma/2(J+\frac{1}{2})]\cdot[(J-\frac{1}{2})(J+\frac{1}{2})-4]$	Lower sign: 0
$\langle^2\Sigma\rvert$	symm		$2\omega_2+B_2(J+\frac{1}{2})(J+\frac{1}{2}\pm 1)\pm\frac{1}{2}\gamma(J+\frac{1}{2}\mp 1)$

Again for the $^2\Sigma$ state, the upper and lower signs correspond to F_1 and F_2 respectively, so that the non-vanishing off-diagonal elements occur only between $^2\Delta(F_1)$ and $^2\Sigma(F_1)$ or between $^2\Delta(F_2)$ and $^2\Sigma(F_2)$. The terms in γ' have been omitted (see text).

Table 10 Matrices for $v_2 = 1$ in a $^3\Sigma$ electronic state

Case (a) representation

	$\lvert {}^3\Pi_2\rangle$	$\lvert {}^3\Pi_1\rangle$	$\lvert {}^3\Pi_0\rangle$
$\langle {}^3\Pi_2 \rvert$	$\gamma'+B_1[J(J+1)-3]+2\lambda-\gamma$	$(\frac{1}{2}\gamma-B_1)\sqrt{2J(J+1)-4}$	$\pm\frac{1}{2}q\sqrt{J(J+1)[J(J+1)-2]}$
$\langle {}^3\Pi_1 \rvert$		$B_1[J(J+1)+1]-2\gamma\pm\frac{1}{2}qJ(J+1)$	$(\frac{1}{2}\gamma-B_1\mp q)\sqrt{2J(J+1)}$
$\langle {}^3\Pi_0 \rvert$	symm		$-\gamma'+B_1[J(J+1)+1]+2\lambda-\gamma\pm q$

$\omega_2 + g_{22} - \frac{4}{3}\lambda$ has been substracted from the diagonal elements. As in Table 9, the basis functions are the Wang 'sum' or 'difference' functions for the upper and lower signs, respectively, for the q terms in the body of the table.

Case (b) representation

	$\lvert N=J+1(F_3)\rangle$	$\lvert N=J(F_2)\rangle$	$\lvert N=J-1(F_1)\rangle$
$\langle N=J+1\rvert$	$[B_1 \pm \frac{1}{2}q-\gamma/(J+1)][J^2+3J+1]\pm\frac{1}{2}q$ $-\frac{2}{3}\lambda(J^2+3J-1)/(J+1)(2J+1)$	$-(\gamma J+2\lambda)\sqrt{J+2}/(J+1)\sqrt{2J+1}$	$-2\lambda\sqrt{(J-1)(J+2)}/(2J+1)$
$\langle N=J\rvert$		$[B\mp\frac{1}{2}q-\gamma/J(J+1)][J^2+J-1]$ $\mp\frac{1}{2}q+\frac{2}{3}\lambda[1-3/J(J+1)]$	$[\gamma(J+1)-2\lambda]\sqrt{J-1}/J\sqrt{2J+1}$
$\langle N=J-1\rvert$	symm		$[B\pm\frac{1}{2}q+\gamma/J][J^2-J-1]\pm\frac{1}{2}q$ $-\frac{2}{3}\lambda(J^2-J-3)/J(2J+1)$

$\omega_2 + g_{22}$ has been subtracted from the diagonal elements, and the terms involving γ' have been omitted.

Table 11 Case (a) and Case (b) matrices for the $v_2=2$ level in $^3\Sigma$ state.

$(^3\Sigma, ^3\Delta)$	$\lvert^3\Delta_3\rangle$	$\lvert^3\Delta_2\rangle$	$\lvert^3\Delta_1\rangle$	$\lvert^3\Sigma_1\rangle$	$\lvert^3\Sigma_0\rangle$
$\langle^3\Delta_3\rvert$	$4g_{22}+B_2[J(J+1)-8]+2\lambda-\gamma$	$(\frac{1}{2}\gamma-B_2)\sqrt{2J(J+1)-12}$	0	$(q/\sqrt{2})\sqrt{J(J+1)-2}\sqrt{J(J+1)-6}$	0
$\langle^3\Delta_2\rvert$		$4g_{22}+B_2[J(J+1)-2]-2\gamma$	$(\frac{1}{2}\gamma-B_2)\sqrt{2J(J+1)-4}$	$-2q\sqrt{J(J+1)-2}$	$q\sqrt{J(J+1)}\sqrt{J(J+1)-2}$
$\langle^3\Delta_1\rvert$			$4g_{22}+B_2J(J+1)+2\lambda-\gamma$	$q\sqrt{2}\{1\pm\frac{1}{2}J(J+1)\}$	$-2q\sqrt{2J(J+1)}$
$\langle^3\Sigma_1\rvert$				$B_2J(J+1)+2\lambda-\gamma$	$2(\frac{1}{2}\gamma-B_2)\sqrt{J(J+1)}$
$\langle^3\Sigma_0\rvert$	symm				$B_2[J(J+1)+2]-2\gamma$

In Table 9 the basis functions are Wang 'sum' functions for the upper 4 signs and 'difference' functions for the lower signs; in the $v_2 = 2$ matrices, the single $|^3\Sigma_0\rangle$ function must be counted with the 'sum' functions giving a 5 x 5 matrix, whereas the 'difference' functions give a 4 x 4 matrix. The quantity $\frac{4}{3}\lambda$ has been subtracted from all diagonal elements.

Case (b) MATRIX

$^3\Delta$ $^3\Sigma$

	|N=J+1>	|N=J>	|N=J-1>	4x4:- |N=J> 5x5:- |N=J+1>	|N=J-1>
<N=J+1|	$2\omega_2+4g_{22}+[B-\frac{\gamma}{(J+1)}][(J+1)(J+2)-4]-\frac{2}{3}\lambda\frac{(J-2)(J+5)}{(J+1)(2J+1)}$	$\frac{2\gamma J+4\lambda}{J+1}\sqrt{\frac{(J-1)(J+3)}{J(2J+1)}}$	$\frac{2\lambda}{2J+1}\sqrt{\frac{(J-1)(J-2)(J+2)(J+3)}{J(J+1)}}$	4x4:- 0 5x5:- $-q\sqrt{J(J+1)(J+2)(J+3)}$	0
<N=J|		$2\omega_2+4g_{22}+\frac{2}{3}\lambda[1-\frac{12}{J(J+1)}]+[B-\frac{\gamma}{J(J+1)}][J(J+1)-4]$	$\frac{2\gamma(J+1)-4\lambda}{J}\sqrt{\frac{(J+2)(J-2)}{(J+1)(2J+1)}}$	4x4:- $-q\sqrt{J(J+1)(J-1)(J+2)}$ 5x5:- 0	0
<N=J-1|			$2\omega_2+4g_{22}-\frac{2}{3}\lambda(\frac{J^2-J-12}{J(2J+1)})+(B+\frac{\gamma}{J})(J^2-J-4)$	4x4:- 0 5x5:- 0	$q\sqrt{J(J+}$ $\sqrt{(J-1)}$ $\sqrt{(J-2)}$
4x4: <N=J|				4x4:- $2\omega_2+BJ(J+1)+\frac{2}{3}\lambda-\gamma$	-2λ $2J+1$
5x5: <N=J+1|				5x5:- $B(J+1)(J+2)+2\omega_2-\gamma(J+2)-\frac{2}{3}\lambda(\frac{J+2}{2J+1})$	$\sqrt{J(J+1)}$
<N=J-1|	symm				$BJ(J-1$ $\gamma J-\frac{2}{3}\lambda$ $\frac{J-1}{2J+1}+$ $2\omega_2$

The 5x5 matrix (Wang 'sum') is Kronig '-' for J even and vice versa for J odd

The 4x4 matrix (Wang 'difference) is Kronig '+' for J even

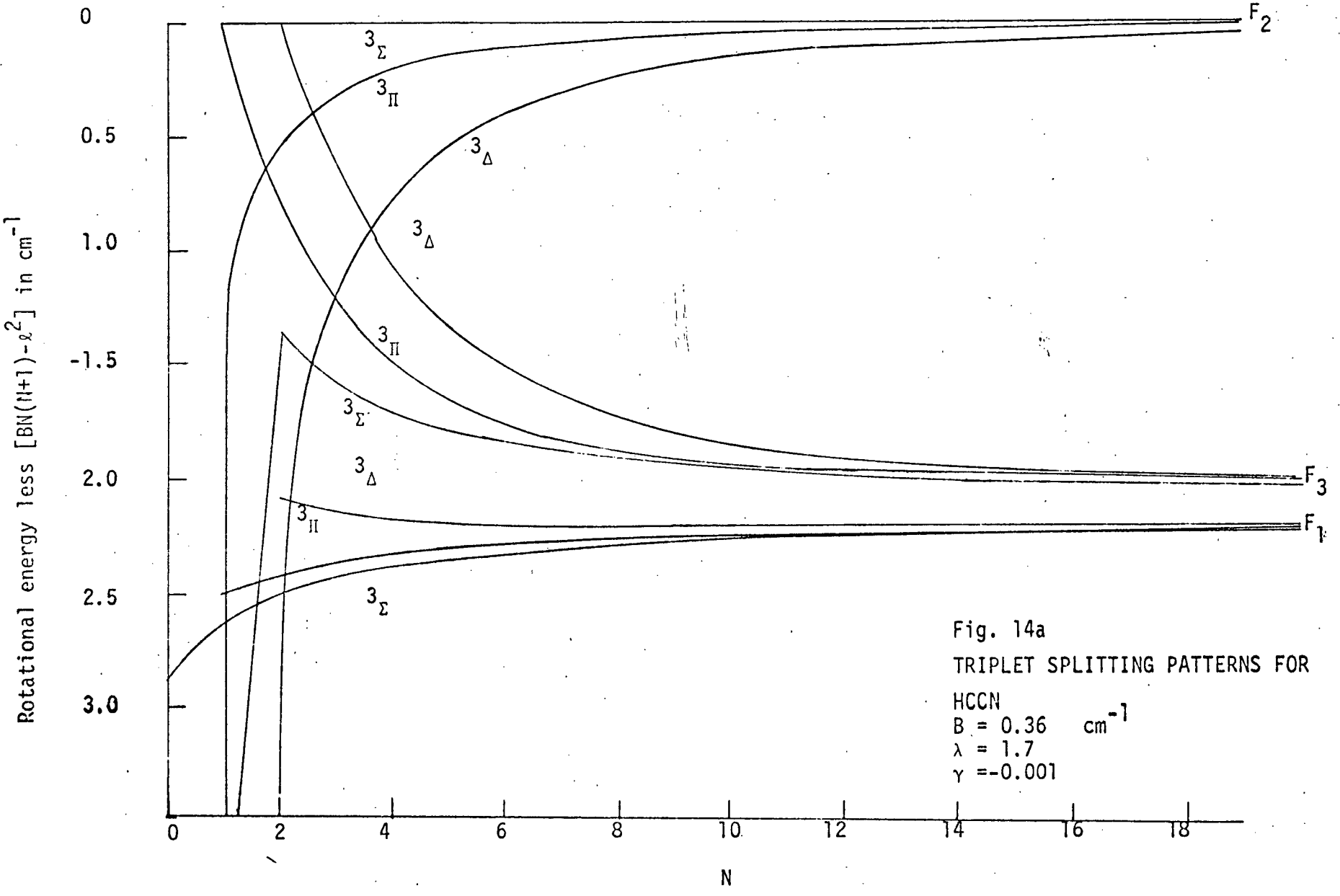

Fig. 14a

TRIPLET SPLITTING PATTERNS FOR

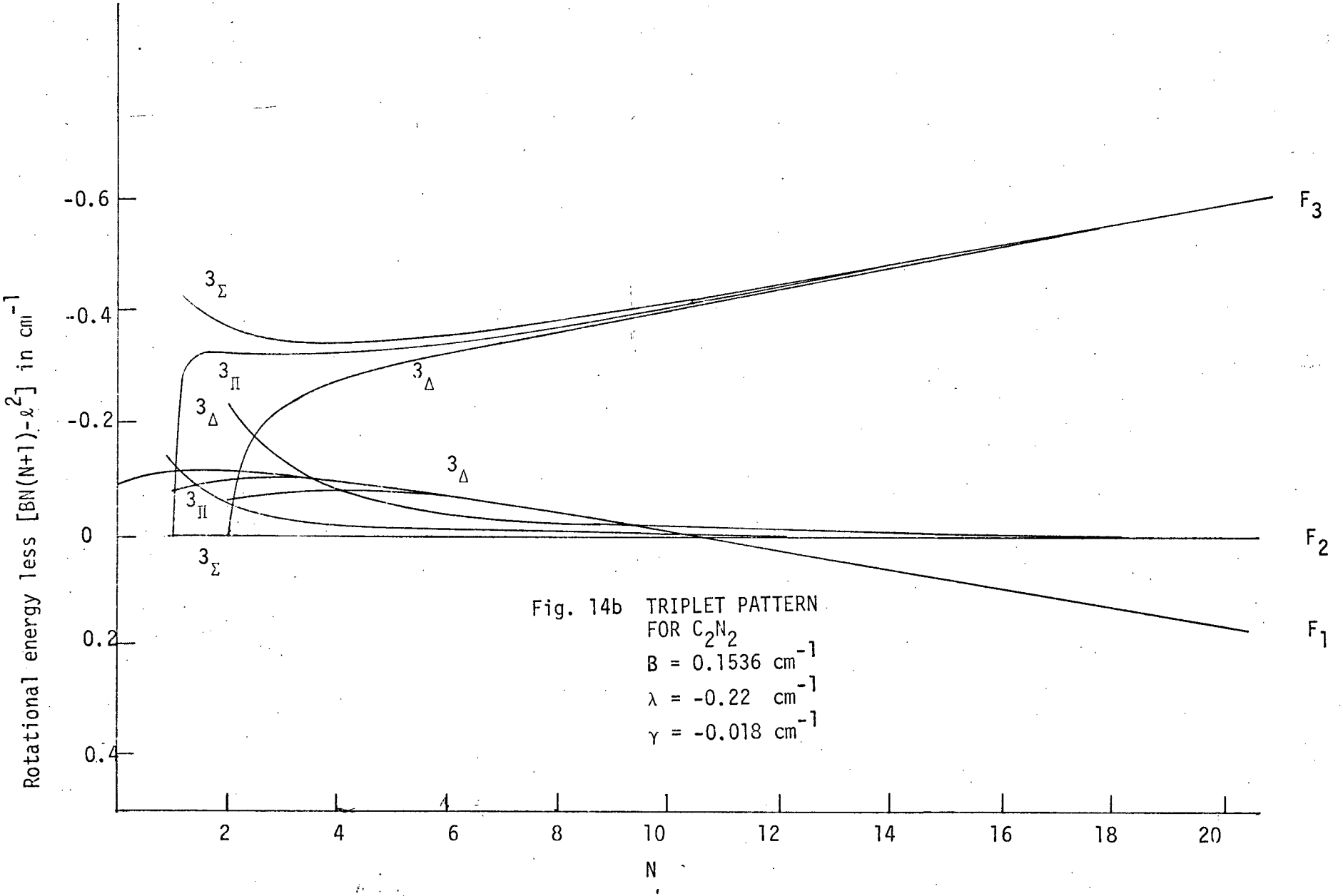

Fig. 14b TRIPLET PATTERN FOR C_2N_2

$B = 0.1536\ cm^{-1}$

$\lambda = -0.22\ cm^{-1}$

$\gamma = -0.018\ cm^{-1}$

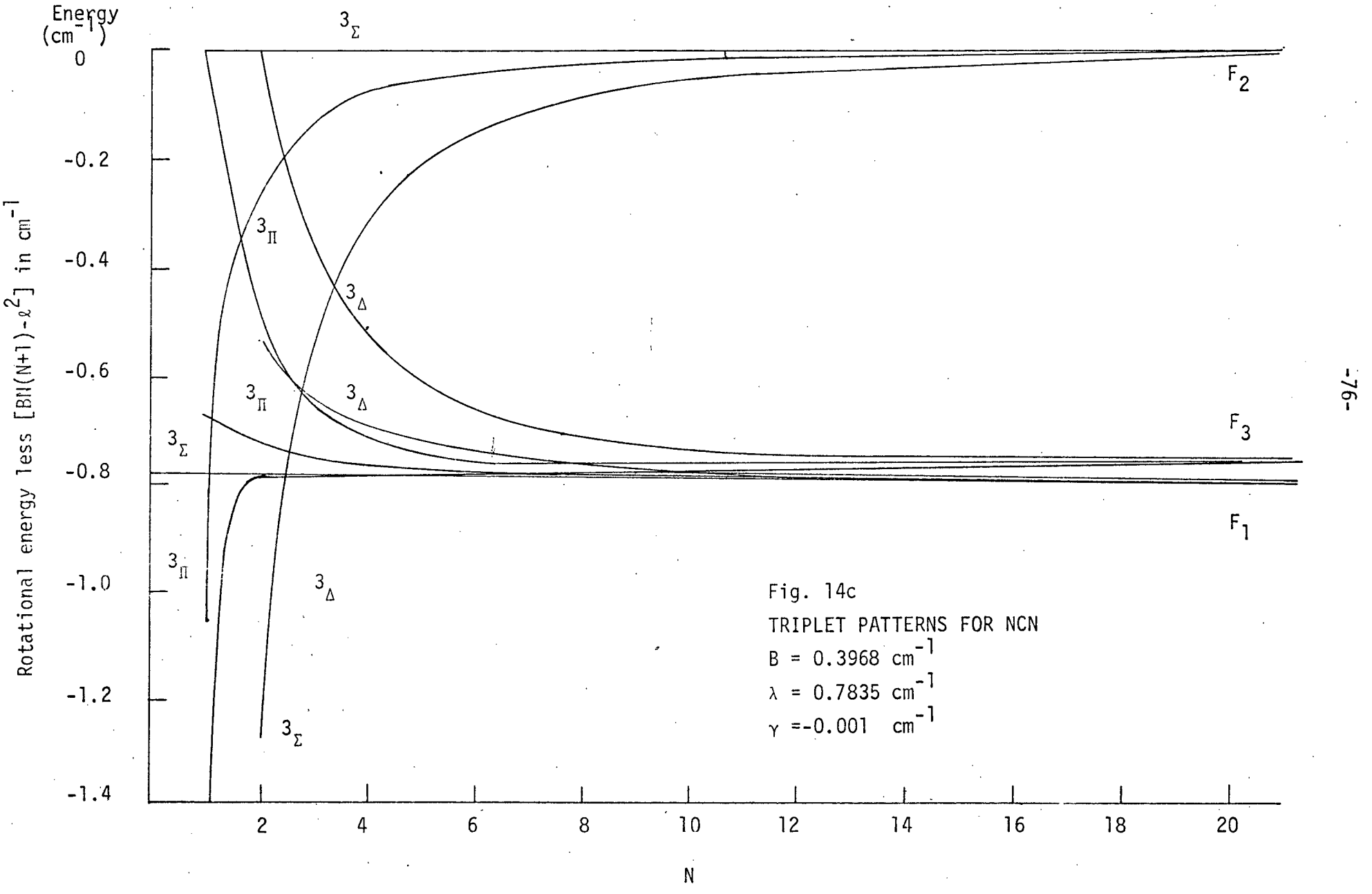

Fig. 14c
TRIPLET PATTERNS FOR NCN
B = 0.3968 cm^{-1}
λ = 0.7835 cm^{-1}
γ =-0.001 cm^{-1}

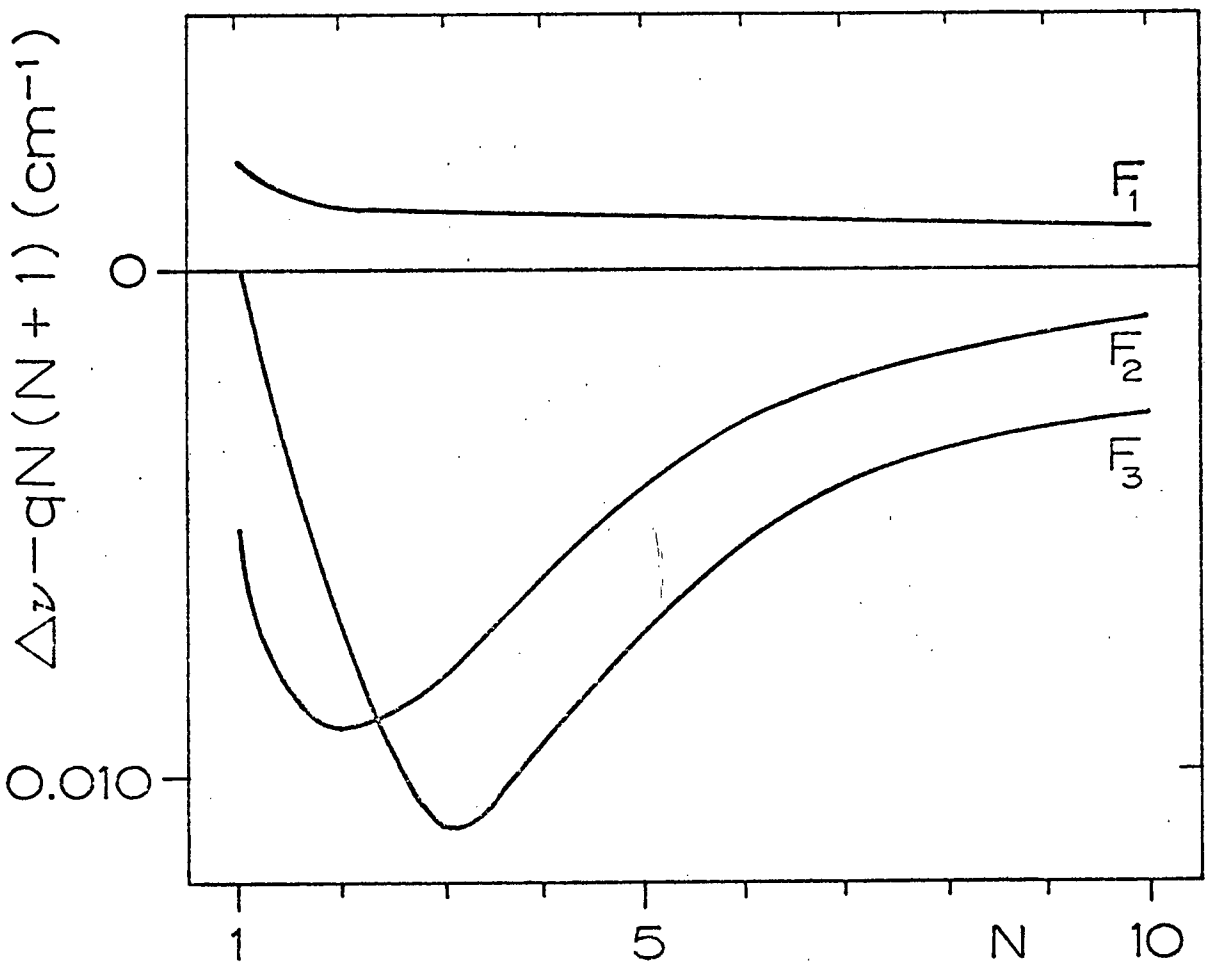

Fig. 15 Departure of the ℓ-type doubling of a hypothetical state of HCCN, with B = 0.36, λ = 1.7, γ = -0.001 and q = 0.003 cm^{-1}, from the case (b) formula $\Delta\nu = qN(N+1)$ for the vibronic $^3\Pi$ level ($v_4 = 1$).

References

1. W.W. Watson and A.E. Parker, Phys. Rev. 37, 1484 (1930).
J.H. Clements, Phys. Rev. 47, 224 (1935).
R.K. Asundi and R. Samuel, Proc. Ind. Acad. Sci. 2A, 30 (1935).
2. N. Metropolis and H. Beutler, Phys. Rev. 57, 1078 (1940).
N. Metropolis, Phys. Rev. 60, 283 (1941).
3. G. Herzberg, Electronic Spectra of Polyatomic Molecules, Van Nostrand, Princeton, New Jersey, U.S.A., pg. 75 (1966).
4. A.J. Merer and D.N. Travis, Canad. J. Phys. 44, 353 (1966).
5. P.W. Schenk, Ber. 65, 94 (1942).
6. M. Becke-Goehring, R. Schwarz, and W. Spress, Z. Anorg. Allg. Chem. 293, 294 (1958).
7. W.H. Kirchhoff, J.A.C.S. 90 2437 (1969).
8. G. Brauer, Preparative Methods of Inorganic Chemistry, Academic Press, New York, 1963.
9. A.J. Barnes and H.E. Hallam, Quarterly Rev. 23, 392 (1969).
10. P.W. Schenk, E. Krow, and H. Kartano-Soeratman, Monatsh 95, 710 (1964).
11. J. White, J. Opt. Soc. Am. 32, 285 (1942).
12. H. Richert, Z. Anorg. Allg. Chem. 309, 171 (1961).
13. J.H. Schachtschneider, Spectrochim, Acta. 19, 117 (1963).
14. E.B. Wilson, J.C. Decius, and P.C. Cross, Molecular Vibrations, McGraw-Hill, New York. 1955.

15. G.M. Barrow, Introduction to Molecular Spectroscopy, McGraw-Hill, New York, 233 (1962).

16. E. Hutchisson, Phys. Rev. 36, 410 (1930).

17. M. Wagner, Z. Naturf. 14a, 81 (1959).

18. F. Ansbacher, Z. Naturf. 14a, 889 (1959).

19. W.L. Smith and P.A. Warsop, Trans. Far. Soc. 65, 1165 (1968).

20. J.B. Coon, R.E. De Wames, and C.M. Lloyd, J. Molec. Spectroscopy 8, 285 (1962).

21. W.L. Smith, J. Phys. B. Proc. Phys. Soc., 2, 1 (1969).

22. R.N. Dixon, private communication.

23. G. Herzberg, Electronic Spectra of Polyatomic Molecules, Van Nostrand, Princeton, New Jersey, U.S.A. (1966).

24. R.T. Birge, Phys. Rev. 25, 240 (1925).

25. A.J. Merer, Disc. Far. Soc. 35, 127 (1963).

26. R.M. Hochstrasser and A.P. Marchetti, J. Mol. Spec. 35, 335 (1970).

27. J.H. Van Vleck, Rev. Mod. Phys. 23, 213 (1951).

28. J.K.G. Watson, Canad. J. Phys. 46, 1637 (1968).

29. C-F. Chang and Y-N. Chiu, J. Chem. Phys. 53, 2186 (1970).

30. J.T. Hougen, The Calculation of Rotational Energy Levels and Line Intensities in Diatomic Molecules. N.B.S. Monograph HS 115, Wash. D.C. U.S.A.

31. J.H. Meal and S.R. Polo, J. Chem. Phys. 24, 1119 (1956).

32. E.B. Wilson, J.C. Decius, and P.C. Cross, Molecular Vibrations, Appendix III McGraw-Hill, New York, 1955.

33. W. Moffitt and A.D. Liehr, Phys. Rev. 106, 1195 (1957).

34. I.M. Mills, Pure and App. Chem. 11, 325 (1965).

35. J.T. Hougen, J. Chem. PHys. 36, 519 (1962).

36. E.C. Kemble, The Fundamentals of Quantum Mechanics, Dover Publications, New York, U.S.A. (1958).

37. S.C. Wang, Phys. Rev. 34, 243 (1929).

38. J.W.C. Johns, Canad. J. Phys. 39, 1739 (1961).

39. J.T. Hougen, Canad. J. Phys. 42, 433 (1964).

40. K.F. Freed, J. Chem. Phys. 45, 4214 (1966).

41. A. Carrington, B.J. Howard, D.H. Levy and J.C. Robertson, Mol. Phys. 15, 187 (1968).

42. J.H. Callomon and A.B. Davey, Proc. Phys. Soc. 83, 335 (1963).

43. G. Herzberg and D.N. Travis, Canad. J. Phys. 43, 353 (1966).

44. R.A. Bernheim, R.J. Kempf, J.V. Gramas and P.S. Skell, J. Chem. Phys. 43, 196 (1965).

45. S.L. Miller and C.H. Townes, Phys. Rev. 90, 537 (1953).

APPENDIX 1

Normal Coordinate Analysis

To solve the vibrational problem in polyatomic molecules, one begins by writing down the hamiltonian using cartesian displacement coordinates for the individual atoms (Δx_1, Δy_1, Δz_1, Δx_2, Δy_2, ... Δz_n) in matrix form

$$H = T + V = \tfrac{1}{2}\, \dot{\underset{\sim}{X}}^{tr}\, \underset{\sim}{M}\, \dot{\underset{\sim}{X}} + \tfrac{1}{2}\, \underset{\sim}{X}^{tr}\, \underset{\sim}{f}\, \underset{\sim}{X} \qquad (1)$$

Here $\underset{\sim}{M}$ is a 3N x 3N (N = number of atoms in the molecule) matrix with the following diagonal form

$$\underset{\sim}{M} = \begin{bmatrix} M_1 & & & & & & \\ & M_1 & & & & & \\ & & M_1 & & & & \\ & & & M_2 & & & \\ & & & & \ddots & & \\ & & & & & \ddots & \\ & & & & & & M_N \end{bmatrix}$$

Since eq. (1) is unwieldly because of the form of the potential energy, one introduces normal coordinates, Q_k, which one defines as fulfilling the following relationship.

$$H = \tfrac{1}{2}\sum_{k}^{3N-6} P_k^2 + \tfrac{1}{2}\sum_{k}^{3N-6} \lambda_k Q_k^2$$
$$= \tfrac{1}{2}\dot{\underset{\sim}{Q}}^{+r}\ \underset{\sim}{E}\ \dot{\underset{\sim}{Q}} + \underset{\sim}{Q}^{+r}\ \underset{\sim}{\Lambda}\ \underset{\sim}{Q} \qquad (3)$$

In this equation P_k is the momentum associated with the normal coordinate, Q_k, and $\underset{\sim}{\Lambda}$ is the diagonal matrix of the eigenvalues corresponding to the observed frequencies ($\Lambda_k = 4\pi^2\nu_k c$, ν_k in cm^{-1}). Notice that k is an index for the normal coordinates.

Now we define the transformation matrix $\underset{\sim}{B}$ that transforms the vector of the cartesian displacement coordinates ($\underset{\sim}{X}$) into the vector of the internal displacement coordinates ($\underset{\sim}{S}$) (changes in bond angles and bond lengths).

$$\underset{\sim}{S} = \underset{\sim}{B}\ \underset{\sim}{X} \qquad (4)$$

Now we define the matrix $\underset{\sim}{G}$ such that

$$\underset{\sim}{G} = \underset{\sim}{B}\ \underset{\sim}{M}^{-1}\ \underset{\sim}{B}^{+r} \qquad (5)$$

and the matrix $\underset{\sim}{L}$ such that

$$\underset{\sim}{S} = \underset{\sim}{L}\ \underset{\sim}{Q} \qquad (6)$$

Now we define the matrix $\underset{\sim}{A}$ such that

$$\underset{\sim}{B}\ \underset{\sim}{A} = \underset{\sim}{E} \qquad (7)$$

The matrix $\underset{\sim}{A}$ is introduced only because $\underset{\sim}{B}$, not being square, lacks a genuine inverse.

Now

$$\underset{\sim}{X} = \underset{\sim}{A}\ \underset{\sim}{S} \qquad (8)$$

and then

$$\underset{\sim}{G}\,\underset{\sim}{G}^{-1} = \underset{\sim}{B}\,\underset{\sim}{M}^{-1}\,\underset{\sim}{B}^{+r}\,\underset{\sim}{G}^{-1} = \underset{\sim}{E} \qquad (9)$$

therefore

$$\underset{\sim}{A} = \underset{\sim}{M}^{-1}\,\underset{\sim}{B}^{+r}\,\underset{\sim}{G}^{-1} \qquad (10)$$

and

$$\underset{\sim}{X} = \underset{\sim}{M}^{-1}\,\underset{\sim}{B}^{+r}\,\underset{\sim}{G}^{-1}\,\underset{\sim}{S} \qquad (11)$$

Now substituting eq. (11) into the first part of eq. (1) one gets

$$2T = \dot{\underset{\sim}{S}}^{tr}\,\underset{\sim}{G}^{-1}\,\dot{\underset{\sim}{S}} \qquad (12)$$

Now using eq. (6) one gets

$$H = \tfrac{1}{2}\,\dot{\underset{\sim}{Q}}^{+r}\,\underset{\sim}{L}^{+r}\,\underset{\sim}{G}^{-1}\,\underset{\sim}{L}\,\dot{\underset{\sim}{Q}} + \tfrac{1}{2}\,\underset{\sim}{Q}^{tr}\,\underset{\sim}{L}^{tr}\,\underset{\sim}{F}\,\underset{\sim}{L}\,\underset{\sim}{Q} \qquad (13)$$

and therefore $\underset{\sim}{L}^{+r}\,\underset{\sim}{G}^{-1}\,\underset{\sim}{L} = \underset{\sim}{E}$ and $\underset{\sim}{L}^{+r}\,\underset{\sim}{F}\,\underset{\sim}{L} = \underset{\sim}{\Lambda}$

or as usually written

$$\underset{\sim}{G}\,\underset{\sim}{F}\,\underset{\sim}{L} = \underset{\sim}{L}\,\underset{\sim}{\Lambda}$$

In principle the unknown $\underset{\sim}{F}$ matrix could be calculated from the $\underset{\sim}{G}$ matrix and the observed frequencies ($\underset{\sim}{\Lambda}$); however, this is computationally difficult. Instead a trial force constant matrix is substituted, the calculated and observed frequencies are compared, and an appropriate adjustment is made to the trial force constant matrix. This process is repeated until a satisfactory agreement between the calculated and observed frequencies is obtained.

APPENDIX 2

The Wang Transformation is a similarity transformation that will break down matrices that are symmetric about both diagonals (doubly symmetric) into smaller sub-matrices. It is equivalent to writing the matrix in terms of a new set of basis functions which are sums and differences of the old basis functions. That is, the Wang Transformation is such that

$$\underset{\sim}{S}\,\underset{\sim}{H}'\,\underset{\sim}{S}^{-1} = H \qquad (1)$$

where H' is doubly symmetric and H consists of two smaller matrices. One should note that the important thing for this thesis is that the pre-transformed basis functions $|\ell,\Sigma>$ are neither symmetric nor antisymmetric under the symmetry operation, σ_v, but the "Wanged" basis functions, which are now sums and differences of the old basis functions, have the required symmetry properties.

The Wang Transformation is shown below for both a 3 x 3 and 4 x 4 matrix.

3 x 3

$$\frac{1}{\sqrt{2}}\begin{vmatrix} 1 & 0 & 1 \\ 0 & \sqrt{2} & 0 \\ -1 & 0 & 1 \end{vmatrix}\begin{vmatrix} A & C & D \\ C & B & C \\ D & C & A \end{vmatrix}\frac{1}{\sqrt{2}}\begin{vmatrix} 1 & 0 & -1 \\ 0 & \sqrt{2} & 0 \\ 1 & 0 & 0 \end{vmatrix}$$

$$= \begin{vmatrix} A-D & 0 & 0 \\ 0 & B & \sqrt{2}\,C \\ 0 & \sqrt{2}\,C & A+D \end{vmatrix} = [A-D] + \begin{vmatrix} B & \sqrt{2}\,C \\ \sqrt{2}\,C & A+D \end{vmatrix}$$

4 x 4

$$\frac{1}{\sqrt{2}}\begin{vmatrix} 1 & 0 & 0 & 1 \\ 0 & 1 & 1 & 0 \\ 0 & -1 & 1 & 0 \\ -1 & 0 & 0 & 1 \end{vmatrix}\begin{vmatrix} A & C & E & F \\ C & B & D & E \\ E & D & B & C \\ F & E & C & A \end{vmatrix}\frac{1}{\sqrt{2}}\begin{vmatrix} 1 & 0 & 0 & -1 \\ 0 & 1 & -1 & 0 \\ 0 & 1 & 1 & 0 \\ 1 & 0 & 0 & 1 \end{vmatrix}$$

$$= \begin{vmatrix} A-F & C-E & 0 & 0 \\ C-E & B-D & 0 & 0 \\ 0 & 0 & B+D & C+E \\ 0 & 0 & C+E & A+F \end{vmatrix}$$

$$= \begin{vmatrix} A \pm F & C \pm E \\ C \pm E & B \pm D \end{vmatrix}$$